HHS Public Access

Author manuscript

Nature. Author manuscript; available in PMC 2019 May 28.

Published in final edited form as:

Nature. 2019 January ; 565(7737): 96–100. doi:10.1038/s41586-018-0749-z.

Metabolic reprogramming by the S-nitroso-CoA Reductase system protects from kidney injury

Hua-Lin Zhou[1], **Rongli Zhang**[#1], **Puneet Anand**[#1], **Colin T. Stomberski**[1], **Zhaoxia Qian**[1], **Alfred Hausladen**[1], **Liwen Wang**[2], **Eugene P. Rhee**[3,4], **Samir M. Parikh**[5,6], **S. Ananth Karumanchi**[5,6,7], and **Jonathan S. Stamler**[1,8,*]

[1]Institute for Transformative Molecular Medicine and Department of Medicine, Case Western Reserve University and University Hospitals Cleveland Medical Center, Cleveland, Ohio 44106, USA,

[2]Center for Proteomics and Bioinformatics, Case Western Reserve University School of Medicine, Cleveland, Ohio 44106, USA.

[3]Nephrology and Endocrine Divisions, Massachusetts General Hospital and Harvard Medical School, Boston, Massachusetts 02114, USA.

[4]Broad Institute of MIT and Harvard, Cambridge, Massachusetts 02139, USA.

[5]Division of Nephrology and Department of Medicine, Beth Israel Deaconess Medical Center and Harvard Medical School, Boston, Massachusetts 02215, USA.

[6]Center for Vascular Biology Research, Beth Israel Deaconess Medical Center and Harvard Medical School, Boston, Massachusetts 02215, USA.

[7]Department of Medicine, Cedars-Sinai Medical Center, Los Angeles, California, 90048, USA

[8]Harrington Discovery Institute, University Hospitals Cleveland Medical Center, Cleveland, Ohio 44106, USA.

[#] These authors contributed equally to this work.

Abstract

[*]Materials & Correspondence: Institute for Transformative Molecular Medicine, Case Western Reserve University, Wolstein Research Building 4129, 2103 Cornell Road, Cleveland, OH 44106, Tel.: 216-368-5725, Fax: 216-368-2968, jonathan.stamler@case.edu. Correspondence and requests for materials should be addressed to J.S.S (jonathan.stamler@case.edu).

Author contributions

H.Z. and J.S.S. designed the study. H.Z. carried out most of experiments and analyzed the results. R.Z. performed AKI surgery. P.A. prepared samples for iTRAQ LC-MS/MS and metabolomics. C.T.S. prepared samples for photolysis-chemiluminescence assay. A.H. and P.A. purified SCoR from bovine kidney. Z.Q. handled mice. L.W. performed quantitative iTRAQ LC-MS/MS. E. R. and S. M. P. contributed to project conception and carried out metabolomics analyses. S.A.K. contributed to project conception and performed histological stains. H.Z. and J.S.S. wrote the manuscript with input from all authors.

Data availability

The authors declare that the data supporting the findings of this study are available within the paper and its supplementary information files. All data sets generated and/or analyzed in the current study are available from the corresponding author upon reasonable request. Supplementary fig.1 contains scanned complete images of western blots. All experimental data from mice models are provided in the source data file.

The authors declare no competing interests.

Endothelial nitric oxide (NO) synthase (eNOS) is protective against kidney injury, but the molecular mechanisms are poorly understood[1,2]. NO-based cellular signaling is generally mediated by protein S-nitrosylation, the oxidative modification of Cys residues to form S-nitrosothiols (SNOs). S-nitrosylation regulates proteins in all functional classes, and is controlled by enzymatic machinery including S-nitrosylases and denitrosylases that add and remove SNO from proteins, respectively[3,4]. We recently reported in *Saccharomyces cerevisiae* that the classic metabolic intermediate Co-enzymeA (CoA) serves as an endogenous source of SNOs through its conjugation with NO to form S-nitroso-CoA (SNO-CoA), and that S-nitrosylation of proteins by SNO-CoA is governed by its cognate denitrosylase, SNO-CoA reductase (SCoR)[5]. Mammals possess a functional homologue of yeast SCoR, an aldo-keto reductase family member (AKR1A1)[5] with an unknown physiological role. Here we report that the SNO-CoA/AKR1A1 (SCoR) system is highly expressed in renal proximal tubules where it transduces the activity of eNOS in reprogramming intermediary metabolism, thereby protecting kidneys from acute kidney injury (AKI). Specifically, AKR1A1 deletion in mice to reduce SCoR activity increased protein S-nitrosylation, protected against AKI and improved survival, whereas renoprotection was lost in *Akr1a1*$^{-/-}$/*eNOS*$^{-/-}$ mice. Metabolic profiling coupled with unbiased mass spectrometry-based SNO-protein identification revealed that protection by the SNO-CoA/SCoR system is mediated by inhibitory S-nitrosylation of pyruvate kinase M2 (PKM2) through a novel locus of regulation, thereby balancing fuel utilization (through glycolysis) with redox protection (through the pentose phosphate shunt). Targeted deletion of PKM2 from mouse proximal tubules recapitulated precisely the protective and mechanistic effects of S-nitrosylation in *Akr1a1*$^{-/-}$ mice, whereas Cys-mutant PKM2 refractory to S-nitrosylation negated SNO-CoA bioactivity. Our discoveries provide a first physiological function of the SNO-CoA/SCoR system in mammals, reveal novel regulation of renal metabolism and of PKM2 in differentiated tissues in particular, and offer a new perspective on kidney injury with therapeutic implications.

Main

SCoR denitrosylases mediate CoA-dependent denitrosylation of proteins (Extended Data Fig.1a&b), but their role in mammals is unknown. We found that SCoR (aka AKR1A1, formally an aldoketoreductase of unknown function) is expressed widely, but most abundantly in proximal tubules (Fig.1a&b). Notably, AKR1A1 constitutes 0.11% of protein in bovine kidney (Extended Data Fig.1c). eNOS is also expressed highly in proximal tubule epithelial cells, and its expression is induced by AKI, whereas nNOS and iNOS are barely detectable (Extended Data Fig.1d-f)[1,6]. To investigate the physiological role of the SNO-CoA/SCoR system, we created AKR1A1-knockout mice (*Akr1a1*$^{-/-}$) (Extended Data Fig. 1g-h), as well as AKR1A1/eNOS double-knockout mice (*Akr1a1*$^{-/-}$/*eNOS*$^{-/-}$). SNO-CoA metabolizing activity was dramatically reduced in the kidneys of both *Akr1a1*$^{-/-}$ and *Akr1a1*$^{-/-}$/*eNOS*$^{-/-}$ mice (Fig.1c&d).

We subjected WT and *Akr1a1*$^{-/-}$ strains to ischemia-reperfusion (I/R) induced AKI. Interestingly, SNO-CoA metabolizing activity was reduced after AKI in WT mice (Extended Data Fig.2a-c). Serum creatinine and blood urea nitrogen (BUN), indicators of kidney dysfunction, were significantly lower in *Akr1a1*$^{-/-}$ than WT (*Akr1a1*$^{+/+}$) mice (Fig.1e&f). Renoprotection in *Akr1a1*$^{-/-}$ mice was lost in *Akr1a1*$^{-/-}$/*eNOS*$^{-/-}$ mice, indicating that

protection by SCoR inhibition is dependent on NO. Conversely, *eNOS*$^{-/-}$ mice were more susceptible to injury than WT, and deletion of AKR1A1 (*Akr1a1*$^{-/-}$/*eNOS*$^{-/-}$) counteracted their vulnerability (Fig.1e&f) (Extended Data Fig.2d), indicating that protection by eNOS is identified with SNO-CoA. Tubular injury was attenuated in *Akr1a1*$^{-/-}$ mice compared with either *Akr1a1*$^{+/+}$ or *Akr1a1*$^{-/-}$/*eNOS*$^{-/-}$ mice (Fig.1g&h) (Extended Data Fig.2e&f). Since *Akr1a1*$^{-/-}$ mice have an ascorbate deficiency[7], chow diet was supplemented with 1% ascorbate, which normalized ascorbate levels, but had no effect on the AKI phenotype (Extended Data Fig.3a-c). Collectively, our data support the novel perspective that protection against AKI by eNOS-derived NO is identified with SNO-CoA bioactivity and governed by SCoR.

Knockout of SCoR improved survival following AKI (Fig.1i). Female *Akr1a1*$^{-/-}$ mice exhibited the same protective phenotype as males, and both male and female *Akr1a1*$^{-/-}$ mice also were protected against lipopolysaccharide (LPS)-induced AKI (Extended Data Fig.3d-i). We found that endogenous SNOs (SNO-proteins) were significantly higher in injured kidneys of *Akr1a1*$^{-/-}$ vs. *Akr1a1*$^{+/+}$ mice (Fig.1j), whereas iron nitrosyl levels (a measure of NO production) were unchanged. These data suggest that protein S-nitrosylation by SNO-CoA protects against AKI.

Protein S-nitrosylation typically operates within multiprotein macro-complexes, where SCoR may interact directly with SNO targets[4,8]. Most targets of SCoR in yeast are metabolic enzymes, and alterations in metabolism after AKI may play a protective role[5,9,10]. Therefore, to identify protein targets of S-nitrosylation that mediate protection by the SNO-CoA/SCoR system, we combined three unbiased proteomic and metabolomic screening approaches. First, resin-assisted capture of SNO-proteins (SNO-RAC) was coupled with quantitative mass spectrometry. SNO-protein levels from injured *Akr1a1*$^{-/-}$ kidneys were elevated versus *Akr1a1*$^{+/+}$ and 45 SNO-proteins were detected as enriched ≥1.4 fold (Fig. 2a&b) (Supplementary Table 1). Second, we isolated the AKR1A1 interactome from mouse kidney extracts by immunoprecipitation, identifying 37 proteins (Supplementary Table 2). Notably, seven proteins overlapped with the nitrosoproteome (SNO-ome) identified by SNO-RAC, including the prominent metabolic enzyme pyruvate kinase M2 (PKM2) (Fig.2c) (Supplementary Table 3). Third, we performed metabolic profiling following AKI (vs. sham) in *Akr1a1*$^{-/-}$ vs. *Akr1a1*$^{+/+}$ mice. Multiple upstream glycolytic intermediates accumulated in injured kidneys of *Akr1a1*$^{-/-}$ mice, whereas downstream intermediates pyruvate and lactate did not accumulate (Fig.2d-i). These data suggest a block at the last step in glycolysis—between PEP and pyruvate—which is catalyzed by PKM2 (Fig.2j) (note: declines in pyruvate are likely prevented via multiple routes, including degradation of amino acids, conversion of lactate to pyruvate, and oxidative decarboxylation of L-malate[11,12]). Thus, PKM2 is identified as: i. a SNO-CoA-regulated SNO-protein, ii. a component of the AKR1A1/SCoR interactome, and iii. a site of metabolic regulation by the SNO-CoA/SCoR system. Our results point to inhibitory S-nitrosylation of PKM2 in injured kidneys of *Akr1a1*$^{-/-}$ mice.

To verify the regulation of PKM2 by SCoR, we measured S-nitrosylated PKM2 (SNO-PKM2) level and activity following AKI. SNO-PKM2 was higher in *Akr1a1*$^{-/-}$ vs. *Akr1a1*$^{+/+}$ kidneys, and increased SNO-PKM2 was associated with lower PKM2 activity;

both increased SNO-PKM2 and decreased PKM2 activity were eNOS-dependent (Fig.3a-c). Increased SNO-PKM2 and decreased PKM2 activity in *Akr1a1*$^{-/-}$ mice were also correlated with protection in endotoxin-induced AKI (Extended Data Fig.3j-l). As further validation, we found that PKM2 interacted with AKR1A1 in HEK cells, as it does in native kidneys, and that recombinant PKM2, but not other PK isoforms (PKM1 or PKLR), was directly inhibited by SNO-CoA (Fig.3d) (Extended Data Fig. 4a&b). Our data indicate that PKM2 activity following AKI is governed by SCoR-regulated S-nitrosylation.

PKM2 has 10 Cys residues and individual mutation revealed that four cysteine residues, C152, C358, C423 and C424, account for measureable S-nitrosylation by eNOS (Extended Data Fig.5a) (Fig.3e). PKM2 degradation was promoted by C152 mutation (Extended Data Fig.5b-e). S-nitrosylation of PKM2 may therefore explain reduced PKM2 expression in *Akr1a1*$^{-/-}$ mice (Fig.3a) (Extended Data Fig.4c&d). Oxidation of PKM2 at C358 can inhibit PKM2 activity[13,14]; however, C423/424 are newly discovered regulatory sites. Interestingly, C423 and C424 are encoded by the PKM2-specific alternative exon 10 and are localized at the interacting surface of the PKM2 tetramer (Extended Data Fig.6a&b). The activity of PKM2-C423/424A cannot be inhibited by SNO-CoA *in vitro* or the NO donor DETA-NO in HEK cells, confirming that cysteines 423/424 are the principal targets of NO (Fig.3f) (Extended Data Fig.7a&b). Using purified proteins, we found that SNO-CoA inhibited formation of tetrameric PKM2-WT but not tetrameric PKM2-C423/424A (Fig.3g). NO promoted the accumulation of PEP in Myc-PKM2-WT but not Myc-PKM2-C423/424A cells (Fig.3h). Thus, S-nitrosylation of C423/424 is primarily responsible for inhibition of PKM2 by SNO-CoA.

We wondered how inhibition of a terminal step in glycolysis could confer protection against AKI. We noted that multiple pentose phosphate pathway (PPP)-related intermediates were increased in *Akr1a1*$^{-/-}$ kidneys following AKI (Fig.4a-d), and that NO promoted accumulation of PPP intermediates in Myc-PKM2-WT vs. Myc-PKM2-C423/424A cells (Extended Data Fig.7d). PPP is a metabolic pathway for generating NADPH[15], which can increase glutathione (GSH) and activate anti-oxidant enzymes, lessening kidney injury[16], and we confirmed that the NADPH/NADP^{+} ratio following AKI was higher in kidneys of *Akr1a1*$^{-/-}$ vs. *Akr1a1*$^{+/+}$ or *Akr1a1*$^{-/-}$/*eNOS*$^{-/-}$ mice (Fig.4e). Thus, inhibitory S-nitrosylation of PKM2 increases flux through the PPP.

Reactive oxygen species (ROS) are central mediators of AKI[17,18], and enhanced antioxidant defenses can ameliorate AKI[19,20]. Tissue indicators of oxidative stress, GSSG (oxidized GSH)/GSH and lipid peroxidation, were lower in injured kidneys of *Akr1a1*$^{-/-}$ mice than in *Akr1a1*$^{+/+}$ or *Akr1a1*$^{-/-}$/*eNOS*$^{-/-}$ mice (Fig.4f&g) (without change in total glutathione; Extended Data Fig.7c). ROS levels may reflect mitochondrial dysfunction. However, levels of multiple TCA cycle intermediates were similar in AKI-injured *Akr1a1*$^{-/-}$ and *Akr1a1*$^{+/+}$ mice, and ADP/ATP ratios were no different in Myc-PKM2-WT vs. Myc-PKM2-C423/424A cells under NO treatment (Extended Data Fig.8a-d). We conclude that inhibition of PKM2 by the SNO-CoA/SCoR system shunts metabolic intermediates through the PPP to alleviate oxidative stress and protect against AKI.

To establish conclusively the importance of PKM2 inhibition in protection against AKI and of metabolic reprogramming (PPP vs. glycolytic flux) in renoprotection, we generated renal tubular epithelial cell-specific PKM2-knockout mice (*Pkm2*$^{-/-}$) (Extended Data Fig.9a). Levels of PKM2 were markedly reduced in kidneys of *Pkm2*$^{-/-}$ mice; however, levels of PKM1 were increased compensatorily (Fig.4h). Overall, pyruvate kinase activity in the kidney was reduced by about 40%, which recapitulates precisely PKM activity in the injured kidneys of *Akr1a1*$^{-/-}$ mice (Fig.3c&4i). Serum creatinine and BUN were significantly lower in *Pkm2*$^{-/-}$ than in WT mice (Fig.4j&k) following AKI, indicative of renoprotection. Histological tubular injury was attenuated in *Pkm2*$^{-/-}$ vs. WT mice (Fig.4l&m). Knockout of PKM2 improved survival (Extended Data Fig.9b). NADPH/$NADP^+$ ratio and PEP levels, but not pyruvate levels, were increased in *Pkm2*$^{-/-}$ vs. WT mice (Fig.4n) (Extended data Fig.9c&d). The GSSG/GSH ratio and lipid peroxidation were lower in injured kidneys of *Pkm2*$^{-/-}$ than WT mice (Fig.4o&p). These results confirm that inhibition of PKM2 shifts metabolic flux from energy-generating (glycolytic) to anti-oxidant (PPP) pathways to protect kidneys from AKI.

The discovery of a physiological function for the SNO-CoA/SCoR system in mammals and in cellular metabolism in particular opens a new field of interdisciplinary inquiry. Notably, our results establish an essential role for SNO-CoA in metabolic regulation. SNO-CoA serves as an endogenous source of NO groups and thus as a newly discovered mediator of protein S-nitrosylation, including of key metabolic enzymes (Supplementary Table 1). By coordinating metabolic flux through glycolysis versus PPP, the SNO-CoA/SCoR system regulates the balance between energy and reducing equivalents to protect against AKI (Fig. 4q). NO regulates glycolysis in neurons and glia, but the mechanism has remained unclear[21–23]. Our findings suggest that SCoR-regulated, SNO-CoA-mediated protein S-nitrosylation may subserve metabolic signaling broadly.

The aldo-keto reductase family 1 member A1 (AKR1A1) has physiologically relevant SNO-CoA reductase activity in mammals, including dozens of SNO substrates. AKR1A1 has a role in ascorbic acid synthesis in rodents[7] and activity against gamma-hydroxybutyric acid (GHB)-related aldehydes *in vitro*[24]. But humans do not synthesize ascorbic acid, and AKR1A1 does not regulate GHB *in vivo* (Extended data Fig.7g)[25]. Therefore, the primary function of AKR1A1 had been a mystery[26]. Our work indicates that the major function of AKR1A/SCoR in mammals is to regulate NO-based metabolic signaling. Notably, eNOS-derived NO had been previously identified with both metabolic regulation and renoprotection[1,2,27], but the molecular mechanisms were poorly understood. Our new findings provide an unanticipated mechanistic basis for eNOS-derived NO protection in the kidney, mediated by SNO-CoA and governed by SCoR (Fig.4q).

Pyruvate kinases catalyze the final step in glycolysis (Fig.2j). PKM1 is expressed in high energy-requiring organs including heart, muscle and brain (Extended Data Fig.6c) as a constitutively active tetramer, whereas PKM2 is expressed primarily in fetal (and tumor) cells, and can shift reversibly between tetramer and lower-activity dimer to reprogram metabolism for growth or survival[13,28,29]. Why PKM2 expresses in some differentiated tissues and predominantly after AKI (Extended Data Fig.10a-c)[9] has been unclear. We now show that PKM2 expression enables protection by metabolic reprogramming. S-nitrosylation

of PKM2 by SNO-CoA forces glucose flux into the PPP to detoxify ROS (Fig.4q). PKM2 inhibition also increases serine synthesis, a precursor for lipids, proteins and nucleotides[30], and serine levels are elevated in *Akr1a1*$^{-/-}$ mice following AKI (Extended Data Fig.7e&f). Therefore, an additional advantage of metabolic programming via PKM2 may be in regenerating tissues following injury. By contrast with reversible regulation of PKM2 in AKI, irreversible PKM2 inactivation is associated with diabetic nephropathy[14]. Thus, inhibition of SCoR and/or PKM2 may be advantageous therapeutically in acute injurious conditions including AKI.

Methods

Mice

Mouse studies were approved by the Case Western Reserve University Institutional Care and Use Committee (IACUC). Housing and procedures complied with the Guide for the Care and Use of Laboratory Animals and the American Veterinary Medical Association guidelines on euthanasia. *Akr1a1*$^{+/-}$ mice were made by Deltagen, Inc. Briefly, to knockout AKR1A1 (SCoR) in ES cells, the *Akr1a1*$^{+/-}$ allele was first created by insertion of a LacZ-Neo cassette in place of exon 2 of the *Akr1a1* gene, disrupting in-frame translation of AKR1A1 (Extended Data Fig.1g&h). F1 mice were generated by breeding chimeric male mice with C57BL/6 females. F2 homozygous mutant mice were produced by intercrossing F1 heterozygous males and females. Wild-type littermates produced by crossing *Akr1a1*$^{+/-}$ and *Akr1a1*$^{+/-}$ were used as breeding pairs to generate control mice (*Akr1a1*$^{+/+}$). To generate AKR1A1 and eNOS double knockout mice (*Akr1a1*$^{-/-}$/*eNOS*$^{-/-}$), male *Akr1a1* mice were crossed with female *eNOS*$^{-/-}$ mice, obtained from Jackson Laboratory. To generate renal tubular epithelial cell-specific PKM2-knockout mice (*Pkm2*$^{fl/fl}$*;KSP-Cre* or *Pkm2*$^{-/-}$), conditional PKM2-knockout mice (*Pkm2*$^{fl/fl}$) were crossed with KSP-Cre mice (both obtained from Jackson Laboratory). Wild-type littermates (*Pkm2*$^{+/+}$*;KSP-Cre*) produced by intercrossing *Pkm2*$^{fl/+}$*;KSP-Cre* parents were used as breeders pairs to generate control mice. *Pkm2*$^{fl/fl}$ mice possess loxP sites flanking exon 10 of the PKM gene, which when deleted forces PKM transcripts to splice as PKM1[31]. In *KSP-Cre* mice, the cadherin 16 promoter drives Cre to specifically express in epithelial cells of renal tubules[32]. Genotyping of *Akr1a1*$^{+/+}$ and AKR1A1$^{-/-}$ mice was performed according to the PCR protocol from Deltagen using the following primers: Common forward: `5′-GCAGAGATTCAACAAGTCTCCCCTC-3′`; Mutant reverse: `5′-GGGCCAGCTCATTCCTCCCACTCAT-3′`; Common reverse: `5′-AGCTAAGGCTCCGAGCAGTGCTAAC-3′`. Genotyping of *Akr1a1*$^{-/-}$/*eNOS*$^{-/-}$ mice and *Pkm2*$^{-/-}$ mice was performed according to the PCR protocol from Jackson lab using the following primers: e*NOS*$^{-/-}$ mutant forward: `5′-AATTCGCCAATGACAAGACG-3′`; *eNOS*$^{-/-}$ wild-type forward: `5′-AGGGGAACAAGCCCAGTAGT-3′`; *eNOS*$^{-/-}$ common reverse: `5′-CTTGTCCCCTAGGCACCTCT-3′`; *Pkm2*$^{fl/fl}$ forward: `5′-CCTTCAGGAAGACAGCCAAG-3′`; *Pkm2*$^{fl/fl}$ reverse: `5′-AGTGCTGCCTGGAATCCTCT-3′`; *KSP-Cre* forward: `5′-GCAGATCTGGCTCTCCAAAG-3′`; *KSP-Cre* reverse: `5′-AGGCAAATTTTGGTGTACGG-3′`.

Acute Kidney Injury (AKI)

AKI surgery was carried out as described previously[33]. Mice of similar age (9–11 weeks) and body weight (male: 25–28 g; female: 22–25 g) were used for surgery. The mice were anesthetized with isoflurane (1–3%) in oxygen and then anesthesia was maintained by adjusting isoflurane (0.75–2.0%) as needed. The fur in the surgical area was removed with clippers and the skin sterilized with 3 times alternating washes of betadine (or chlorhexidine) and alcohol. The mouse was placed on a thermostatic station during surgery. The skin and muscle were cut open along the back to expose both right and left kidneys. Gentle blunt dissection revealed the kidney and a Q-tip was used to mobilize and exteriorize the kidney. A 5–0 silk suture was used to clamp the pedicle to block the blood flow to the kidney to induce renal ischemia for 23 min in male mice or 50 min in female mice, then the sutures released to allow reperfusion. The identical steps were performed on both kidneys. A silk suture was used to close the muscle layer of the incision followed by the closure of the skin wound with vicryl. Immediately after the wound closure, 10–20 ml/kg sterile saline was given intraperitoneally to each mouse. The animal was then kept on a heating pad until it gained full consciousness before being returned to home cage. Mice subjected to surgery without clamping the pedicle were used as sham controls. Mortality at 24 hours after AKI for WT, *Akr1a1*$^{-/-}$, *Akr1a1*$^{-/-}$/*eNOS*$^{-/-}$ and *eNOS*$^{-/-}$ mice is shown in Extended Data Fig2.g. Serum creatinine and BUN were determined after 24 hrs of reperfusion upon removal of the kidney (when larger volumes of blood can be collected). Serum creatinine and BUN were measured at University Hospital's Clinical Laboratories.

For the LPS-induced AKI model, LPS (O111:B4, sigma) in saline (0.9%) was injected intraperitoneally to each mouse (10 mg/kg). Immediately after the injection of LPS, 20 ml/kg sterile saline was given intraperitoneally to each mouse. Serum creatinine and BUN were determined after 16 hrs.

SNO-RAC

SNO-RAC was carried out as described previously[34]. Mouse kidneys were mechanically homogenized in lysis buffer (1 mg/5 μl lysis buffer) containing 100 mM Hepes/1 mM EDTA/ 100 μM neocuproine (HEN), 50 mM NaCl, 0.1% (vol/vol) Nonidet P-40, the thiol-blocking agent 0.2% S-methylmethanethiosulfonate (MMTS), 1 mM PMSF and protease inhibitors (Roche). After centrifugation (20,000g, 4 °C, 20 min, ×2), SDS and MMTS were added to the supernatants to 2.5% and 0.2% respectively, and incubated at 50 °C for 20 min. Proteins were precipitated with −20 °C acetone, and re-dissolved in 1 mL of HEN/1% SDS. Precipitation of proteins were repeated with −20 °C acetone, and the final pellets were resuspended in HEN/1% SDS and protein concentrations determined using the Bicinchoninic Acid (BCA) method. Total lysates (2 mg) were incubated with freshly prepared 50 mM ascorbate and 50 μl thiopropyl-Sepharose (50% slurry) and rotated end-over-end in the dark for 4 h. The bound SNO proteins were sequentially washed with HEN/1% SDS and 10% HEN/0.1% SDS; SNO proteins were then eluted with 10% HEN/1% SDS/10% β-meracaptoethanol and analyzed by SDS/PAGE and immunoblotting.

iTRAQ-Coupled SNO-RAC

iTRAQ-Coupled SNO-RAC was carried out as described previously[5]. Extracts of kidney were prepared, and SNO-RAC (4 mg of protein per sample) was carried out as described above. SDS/PAGE gels were Coomassie-blue stained, and lanes were separated into eight segments top-to-bottom and collected in two 1.5 ml tubes. 500 μl of 50% Acetonitrile (ACN)/50% 100 mM ammonium bicarbonate were used to wash gel bands for more than 5 hours while vortexing. After removal of washing buffer, 400 μl of 100% acetonitrile was added to gel pieces and vortexed for 10min. After removal of ACN, gel pieces were dried in a speed vacuum dryer for 10 mins. 200 μl of 10 mM dithiothreitol (DTT) were added to dry gel pieces and vortexed for 45 mins. 200 μl of 55 mM iodoacetamide (IAA) were added to the gel pieces after removal of DTT buffer, incubating for 45 min at dark. After removal of IAA buffer, 400 μl of 1x iTRAQ dissolution solution and 400 μl ACN were used to wash the gel pieces alternatively for two times. Gel pieces were dried for 10 min in a speed vacuum dryer. 500 ng trypsin in 150 μl 1x iTRAQ buffer were added to dried gel pieces on ice for 30 mins, and then incubated overnight at 37°C. Supernatant from the digested protein solution was transferred to a 1.5 ml tube using gel-loading tips. 200 μl extraction buffer of 60% ACN/5% formic acid were added to gel pieces, vortexed for 30 min, and sonicated for 15 min. The supernatant containing peptide extracts was transferred to 1.5 ml tube, and extractions were repeated two more times. The final digested solution was dried completely. iTRAQ labeling was performed according to the instructions of iTRAQ® Reagents - 4plex Applications Kit. Briefly, 30 μl of iTRAQ dissolution buffer (10x) was added to each sample tube (pH > 7), and then iTraq labeling reagents (114, 115, 116, 117) to separate sample tubes: one reagent to one sample tube. Labeling reactions were vortexed for more than 5 hours at room temperature to ensure complete labeling efficiency. The four labeled samples were mixed together and dried. 160 μl of 5% ACN containing 0.5% TFA was added to the mixed labeled sample and cleaned using C18 ziptips. Briefly, C18 tips were wetted 5 times by 20 μl of 50% ACN each time, equilibrated by 100 μl of 5% ACN containing 0.5% TFA. Samples were then loaded to the tip by drawing and expelling 50 cycles to ensure complete binding. The tips were then washed by 20 μl of 5% ACN containing 0.5% TFA 10 times. Peptides were eluted from tips by 20 μl of 60% ACN containing 0.1% Formic Acid three times, eluates combined, and dried for LC-MS/MS Analysis.

Immunoprecipitation

15 μg of AKR1A1 polyclonal antibody (Proteintech) was incubated with 50 μl Protein G Sepharose (GE) (1:1 slurry) at 4 °C overnight. After washing with NETN buffer [150 mM NaCl, 20 mM Tris-Cl (pH 8.0), 0.5 mM EDTA, 0.5 % (v/v) Nonidet P-40 (NP-40), 1mM PMSF and protease inhibitors cocktail)] three times, AKR1A1 antibody bound to Protein G Sepharose was ready for immunoprecipitation. Mouse kidneys were mechanically homogenized in EBC lysis buffer [120 mM NaCl, 20 mM Tris-Cl (pH 8.0), 0.5 mM EDTA, 0.5 % (v/v) NP-40, 1 mM PMSF and protease inhibitors cocktail (1 mg tissue/5 μl lysis buffer)]. After centrifugation (20,000g, 4 °C, 20 min, ×2), 2 ml (2 mg/ml) supernatant was pre-cleared by incubation with 50 μl Protein G Sepharose (1:1 slurry) for 1 hour at 4 °C. After spin down at 1000 g for 1 min, the supernatant was transferred into new tubes and incubated with 50 μl anti AKR1A1 antibody-Protein G Sepharose (1:1 slurry) for 5 hours at 4 °C. Beads were washed by NETN buffer and proteins were eluted with 50 μl 0.1 M glycine

(pH 2.5) for 10 min at room temperature with shaking. Following centrifugation at 1000 g for 2 min, the elution was neutralized by the addition of 5 μl Tris-HCl (1.0 M), pH 8.0. Proteins were identified by LC-MS/MS Analysis. Coimmunoprecipitation (co-IP) was carried out in HEK cells overexpressing V5-AKR1A1 and Myc-PKM2, by co-transfection using Lipofectamine 2000. Cells were collected and lysed in EBC lysis buffer. Anti-Myc affinity gel (Sigma) was used for Co-IP.

LC-MS/MS Analysis

Digested peptides were separated by a UPLC (Waters, Milford, MA) with a Nano-ACQUITY UPLC BEH300 C18 column. Separated peptides were continuously injected into an Orbitrap Elite hybrid mass spectrometer (Thermo Finnigan, San Jose, CA) by a nanospray emitter (10 μm, New Objective). A linear gradient using mobile phase A (0.1% formic acid in water) and B (100% acetonitrile) was used at a flow rate of 0.3 μl/min, starting with 1% mobile phase B and increasing to 40% B at 65 min for protein interaction identification, or increasing to 40% B at 130 min for iTRAQ experiments. All mass spectrometry data were acquired in positive ion mode. For protein interaction identification, a full MS scan (m/z 350–1800) at resolution of 120,000 was conducted, twenty MS2 scans (m/z 350–1800) were selected from twenty most intense peptide peaks of full MS scans. CID cleavage mode was performed at normalized collision energy of 35%. For iTRAQ experiments, a full MS scan (m/z 300–1800) at resolution of 120,000 was conducted, ten MS2 scans (m/z 100–1600) were activated from five most intense peptide peaks of full MS scans. CID and HCD cleavage modes were performed alternatively of the same peptides selected from full MS scans. MS2 resolution of HCD is 15,000. Bioinformatic software MassMatrix was used to search MS data against a database composed of sequences of mouse proteins from Uniprot and their reversed sequences as a decoy database. Modifications including oxidation of methionine and labeling of cysteine (IA modifications) were selected as variable modifications in searching. For iTRAQ labeling searching, MS tag of N terminus, Lys and/or Tyr were selected as variable modification to test labeling efficiency and fixed modification for iTRAQ quantitation analysis. Trypsin was selected as the in-silico enzyme to cleave proteins after Lys and Arg. Precursor ion searching was within 10 ppm mass accuracy and product ions within 0.8 Da for CID cleavage mode and 0.02 Da for HCD cleavage mode. 95% confidence interval was required for protein identification.

Cloning, Expression, and Purification of Recombinant PKM2

The mammalian cell expression plasmid pCMV-PKM2 (Human) was obtained from Origene. Mammalian cell expression plasmid pcDNA-AKR1A1 was constructed by PCR-cloning of human AKR1A1. pCMV-PKM2 cysteine mutants were generated by QuikChange II Site-Directed Mutagenesis Kit (Agilent). For purification of recombinant PKM2, cDNA encoding PKM2-WT or PKM2-C423A/424A were cloned into pET21b (Novagen) to introduce a C-terminal 6xHis tag on the expressed protein. The recombinant PKM2 proteins were purified from BL21-CodonPlus Competent *E. coli* Cells (Agilent). Overnight *E. coli* cultures were sub-cultured into 1 L of LB medium at 5%. At OD600 of 0.5, cultures were induced with 100 mM IPTG and grown for a further 4 hr at 28 °C. Cultures were centrifuged at 4000g for 10 min to harvest the cells. Cell pellets from 1 L cultures were lysed in 10 mL of 1 x PBS buffer containing 1 mM PMSF and protease-inhibitor cocktail by sonication.

After centrifugation at 14500g for 20 min, the supernatant was collected. The lysate was diluted in 30 ml 1 x PBS buffer containing 1mM PMSF and protease-inhibitor cocktail and incubated with 1 mL of Ni-NTA agarose at 4°C for 1 hr with rotation. The slurry was then poured into empty PD-10 columns (GE Healthcare). The beads were washed with 100 mL of 50 mM NaH_2PO_4, 300 mM NaCl buffer containing 20 mM imidazole. Elution was done in 2 mL of 50 mM NaH_2PO_4, 300 mM NaCl buffer with 250 mM imidazole. Buffer was exchanged with modified Roeder D [(20 mM HEPES (pH 7.9), 20% (v/v) glycerol, 0.1 M KCL, 0.2 mM EDTA)] through Microcon centrifugal filter device (Millipore).

Cell culture, siRNA and related treatments

HEK cell transfection was described previously[35]. siRNA-mediated protein depletion was performed in HEK cells. Two custom PKM2 siRNAs that target the 3' UTR of human PKM2 (`5′ CCAGAUGGCAAGAGGGUG 3′` and `5′ GAUCAACGCCUCACUGAAA 3′`) were obtained from Dharmacon. siRNA oligonucleotides (60 pmol/10cm plate) were transfected into HEK cells using Lipofectamine RNAiMAX (Invitrogen) according to the manufacturer's protocol. After 24 hours, 5 μg pCMV-control, pCMV-PKM2-WT or pCMV-PKM2-C423A/424A were co-transfected with siRNA oligonucleotides (60 pmol/10cm plate) into HEK cells using Lipofectamine 2000. After 24 hrs, cells were treated with 500 μM DETA-NO for 20 hr. Cells were then collected for assay.

Pyruvate, GHB, PEP, 6PG, ATP, ADP and serine measurement

The amount of pyruvate was measured using Pyruvate Assay Kit (Sigma). Kidneys harvested from *Akr1a1*$^{+/+}$, *Akr1a1*$^{-/-}$, *Pkm2*$^{+/+}$ or *Pkm2*$^{-/-}$ mice (sham operation or AKI) were mechanically homogenized in Pyruvate Assay Buffer (1 mg/5 μl buffer). After extracts were clarified by centrifugation (20,000g, 4 °C, 20 min, ×2), supernatant was used for assay. GHB in the serum of *Akr1a1*$^{+/+}$ and *Akr1a1*$^{-/-}$ mice was measured following the GHB enzymatic assay kit from BUHLMANN. For measuring PEP, 6PG, ATP, ADP and serine in HEK cells, 1×10^6 cells were lysed in corresponding buffer. The amount of PEP, 6PG, ATP, ADP and serine were respectively measured using PEP Colorimetric/Fluorometric Assay Kit (Sigma), 6 Phosphogluconate Assay kit (abcam), ATP Colorimetric/Fluorometric Assay Kit (Sigma), ADP Colorimetric/Fluorometric Assay Kit (Sigma) and DL-Serine Assay kit (Fluorometric) (Biovision).

Assay of NADPH-dependent SNO-CoA Reductase activity in Mouse.

Kidneys harvested from *Akr1a1*$^{+/+}$, *Akr1a1*$^{-/-}$ and *Akr1a1*$^{-/-}$/*eNOS*$^{-/-}$ mice were mechanically homogenized in lysis buffer [50 mM phosphate buffer, pH 7.0, 150 mM NaCl, 0.1 mM EDTA, 0.1 mM DTPA, 1 mM PMSF, and protease inhibitor mixture (Roche)]. Extracts were clarified by centrifugation (20,000g, 4 °C, 20 min, ×2), and protein concentration was determined by bicinchoninic acid assay. The NADPH-dependent SNO-CoA reductase activity was determined spectrophotometrically as described previously[5]. Briefly, the assays were performed in 50 mM phosphate buffer (pH 7.0; containing 0.1 mM EDTA and DTPA) with 0.2 mM SNO-CoA and 0.1 mM NADPH. Reactions were initiated by the addition of lysate and allowed to proceed for 1 min. All assays were performed in triplicate.

Photolysis-Chemiluminescence

Kidneys harvested from *Akr1a1*$^{+/+}$ and *Akr1a1*$^{-/-}$ mice were mechanically homogenized in lysis buffer [50 mM phosphate buffer, pH 7.0, 150 mM NaCl, 0.1 mM EDTA, 0.1 mM DTPA, 1 mM PMSF, and protease inhibitor mixture (Roche)]. Extracts were clarified by centrifugation (20,000g, 4 °C, 20 min, ×2), and protein concentration was determined by bicinchoninic acid assay. Measurements of XNO/SNO (where XNO is predominantly metal-NO (MNO)) in lysates were done using photolysis/chemiluminescence essentially as described[36]. Briefly, nitric oxide (NO) released from MNO/SNO by UV-photolysis is detected by chemiluminescence generated by the reaction of NO with ozone. Pre-treatment of samples with $HgCl_2$ (1 mM) (Hg^{2+}-coupled photolysis/chemiluminescence) removes SNO specifically and allows differentiation between SNO and other photolyzable NO species (predominantly MNO).

Histological analysis

Kidney samples were fixed with 4% PFA over 24h, dehydrated and embedded into paraffin blocks. Formalin-fixed, paraffin-embedded blocks were sectioned and stained with Hematoxylin and Eosin stain (H&E). Paraffin-embedded renal tissues were serially sectioned. For immunohistochemistry staining, paraffin sections were dewaxed and rehydrated. Antigen retrieval was performed by boiling sections in 0.01 M sodium citrate buffer (pH 6.0) for 20 min, then sections were washed three times with PBS. Rabbit polyclonal Anti-AKR1A1 (15054–1-AP, Proteintech Group, 1:100) or rabbit polyclonal anti-PKM2 (ABS245, EMD Millipore, 1:100 was dropped onto sections and incubated at 4°C overnight. After washing with PBS, secondary antibody of HRP-associated goat anti-rabbit was dropped and incubated at room temperature for 1 hour. Diaminobenzidine (DAB) was used for coloration. More than ten microscopic fields obtained from each animal were selected for quantitative analysis. Renal histopathologic alterations were evaluated and graded on a 0 to 2 scale as described previously[37,38].

Electron microscopy

Mice were perfused transcardially with quarter-strength Karnovsky's fixative solution at a flow rate of 10 mL/min for 10 minutes. Small pieces of the kidney tissues were immersed in triple aldehyde-DMSO[39]. After rinsing in 0.1 M phosphate buffer (pH 7.3), they were post-fixed in ferrocyanide-reduced osmium tetroxide. Another water rinse was followed by an overnight soak in acidified uranyl acetate. After again rinsing in distilled water, the tissue blocks were dehydrated in ascending concentrations of ethanol, passed through propylene oxide, and embedded in Poly/Bed resin. Thin sections were sequentially stained with acidified uranyl acetate followed by a modification of Sato's triple lead stain[40]. These sections were examined in a FEI Tecnai Spirit (T12) transmission electron microscope with a Gatan US4000 4kx4k CCD.

Pyruvate kinase (PK) activity

PKM activity was measured based on generation of pyruvate, which was oxidized by pyruvate oxidase to produce color (λ = 570 nm). To measure PKM1, PKLR, PKM2-WT and PKM2-C423A/424A protein activity in vitro, DTT in PKM1 (Sigma) and PKLR (R&D

systems) buffer was removed using Amicon Ultra-0.5 mL Centrifugal Filters. 250 ng recombinant PKM1, PKLR, PKM2-WT and PKM2-C423A/424A proteins were pre-incubated with substrate 2 μl fructose-1,6-bisphosphate (FBP)(250 μM) in 2 ml dialysis buffer [20 mM Tris-HCL (pH 7.9), 20% (v/v) glycerol, 0.1 M KCL, 0.2 mM EDTA], followed by dialysis to remove the free FBP in 2L dialysis buffer. WT-FBP complex or PKM2-C423A/424A-FBP complex was treated with 200–300 μM SNO-CoA for 10 min at room temperature, after which the activity of PKM2-WT and PKM2-C423A/424A was measured. To measure PKM1 and PKLR activity, 10 ng PKM1-FBP complex, PKLR-FBP complex or PKM2-FBP complex were treated with 0, 50, 100, 200 or 300 μM SNO-CoA for 10 min at room temperature prior to assay. To measure PK activity in kidney, kidneys were mechanically homogenized in lysis buffer [50 mM phosphate buffer, pH 7.0, 150 mM NaCl, 0.1 mM EDTA, 0.1 mM DTPA, 1 mM PMSF, and protease inhibitor mixture (Roche)]. Extracts were clarified by centrifugation (20,000g, 4 °C, 20 min, ×2), and protein concentration was determined by bicinchoninic acid assay. 10 μl (0.1 μg/μl) lysate was used to measure PKM2 activity. Assay of PKM2 activity was followed the protocol of Pyruvate Kinase Activity Colorimetric/Fluorometric Assay Kit (Biovision).

PKM2 dimer and tetramer formation

Assay of PKM2 dimer and tetramer *in vitro* follows previous descriptions[41]. In brief, after 40ng PKM2-FBP complex was treated with 200–300μM SNO-CoA for 10 min at room temperature, 5 μl fresh glutaraldehyde (50%) was added to a reaction mixture containing 100mM HEPES (pH 7.5) for 5 min at 37°C. The cross-linking reaction was terminated by addition of 5 μl 1M Tris-HCL (PH 8.0). Assay of PKM2 dimer and tetramer *in situ* was carried out as described previously[14]. DSS (disuccinimidyl suberate; Thermo Scientific) (final 500 μM) was added to cells for 30 min at room temperature to cross-link proteins. Cells were lysed in RIPA Buffer and protein concentration was determined by bicinchoninic acid assay. Equal amounts of protein were separated by 4–20% Criterion™ Precast Midi Protein Gel (BIO-RAD) and monomer, dimer and tetramer forms of PKM2 were detected with PKM2 antibody (sc-365684, Santa Cruz Biotechnology).

Western blot analysis

Proteins were extracted from cells or tissues and subjected to 4–20% Criterion™ Precast Midi Protein Gel electrophoresis. Blotted membranes were incubated overnight at 4°C with primary antibodies, and washed with PBS containing 0.1% Tween-20 before incubation with HRP-conjugated secondary antibody (anti-mouse or anti-rabbit IgG (Promega)) for 1 hr followed by chemiluminescent detection (ECL (GE Healthcare)). Antibodies employed in western blotting included: rabbit polyclonal Anti-AKR1A1 (15054–1-AP, Proteintech Group), rabbit monoclonal Anti-PKM1 (D30G6, Cell Signaling), rabbit monoclonal Anti-PKM2 (D78A4, Cell Signaling), rabbit polyclonal Anti-PKLR (AV41699, Sigma), rabbit Polyclonal Anti-NOS1 (sc-8309, Santa Cruz Biotechnology), rabbit Polyclonal Anti-NOS2 (sc-8310, Santa Cruz Biotechnology), rabbit Polyclonal Anti-NOS3 (sc-654, Santa Cruz Biotechnology), mouse Anti-eNOS(pS1177) (612393, BD Transduction Lab), mouse monoclonal p97 (10R-P104A, Fitzgerald), rabbit monoclonal GAPDH (Ab181602, abcam), mouse monoclonal myc (M047–3, MBL), mouse monoclonal FLAG-M2 (F3165, Sigma),

and mouse monoclonal V5 (R960–25, Invitrogen). Quantification of western blot was carried out with ImageJ (NIH).

Expression of PKM1, PKM2 and PKLR

To measure of expression of PKM1, PKM2 and PKLR after AKI, the kidney samples were harvested from AKI-injured WT mice at 1, 3 or 7 days. To compare the expression of PKM1, PKM2 and PKLR between the kidneys of *Akr1a1*$^{+/+}$ and of *Akr1a1*$^{-/-}$ mice, kidney samples were harvested after 24-hours of AKI. Kidney samples were mechanically homogenized in lysis buffer [50 mM phosphate buffer, pH 7.0, 150 mM NaCl, 0.1 mM EDTA, 1 mM PMSF, and protease inhibitor mixture (Roche)]. Extracts were clarified by centrifugation (20,000g, 4 °C, 20 min, ×2), and protein concentration was determined by bicinchoninic acid assay. The expression of PKM1, PKM2 and PKLR was examined using western blot.

GSSG/GSH and NADPH/NADP$^+$

GSSG/GSH ratio was assayed using the GSH/GSSG-Glo™ Assay kit from Promega. Mouse kidney samples (20 mg) were mechanically homogenized in 100 μl total Glutathione Lysis Reagent for total glutathione measurement or 100 μl Oxidized Glutathione Lysis Reagent for GSSG measurement. Extracts were clarified by centrifugation (20,000g, 4 °C, 20 min, x2) and 50 μl supernatant was transferred to the plate reader. 50 μl Luciferin Generation Reagent was added to all wells, and assays were mixed and incubated for 30 minutes. 100μl Luciferin Detection Reagent was added to wells followed by mixing. After 15 minutes of incubation, luminescence was measured using a luminometer. NADPH/NADP$^+$ assay was done with NADP/NADPH-Glo™ Assay kit from Promega. Mouse kidney samples (20 mg) were mechanically homogenized in 100 μl of base solution [50 μl 1 × PBS, 0.2 M NaOH, 1% DTAB (dodecyltrimethylammonium bromide)] for NADPH measurement or acid solution (50 μl 1 × PBS, 0.2N HCl, 1% DTAB) for NADP$^+$ measurement. Extracts were clarified by centrifugation (20,000g, 4 °C, 10 min) and 50 μl supernatant was transferred to the plate reader. After incubating samples for 15 minutes at 60°C, 50 μl of 0.25 M Trizma® base (Sigma) was added to acid-treated cells to neutralize the acid or 50 μl of HCl/Trizma® solution (0.4 M HCl and 0.5 M Trizma® base) was added to base-treated samples. 100 μl NADP/NADPH-GloTM Detection Reagent was added to each well. After incubating for 30–60 minutes at room temperature, luminescence was measured using a luminometer.

Lipid peroxidation

Mouse kidney samples (25 mg) were mechanically homogenized in 250 μl of RIPA Buffer (Invitrogen) containing protease inhibitors and 4 μl 2% (w/v) of the lipid antioxidant BHA. After centrifuging the extract at 160 g for 10 minutes at 4°C, the supernatant was used for analysis. For cells, 2×10^7 cells in 1 ml PBS were sonicated on ice for 10 second and the whole homogenate was used in assays. 100 μl of homogenate or 100 μl standard (malondialdehyde) was combined with 10 μl of TCA-TBA-HCl reagent [0.5% (w/v) TBA in 20% (w/v) TCA and 0.33 N HCl] and mixed thoroughly. 1.5 μl 2% (w/v) of the lipid antioxidant BHA was added to prevent lipid peroxidation during the assay. The solution was heated for 15 min in a boiling water bath. After cooling, the flocculent precipitate was removed by centrifugation at 1000g for 10 min. 150 μl sample or standard (in duplicate) was

loaded to the plate reader. The absorbance of the supernatant was measured at 532nm against a blank that contained reagents minus homogenate. Levels of TBARS [malondialdehyde (MDA) equivalent] were determined with a MDA standard curve.

Metabolomics

Metabolic assays were carried out as described previously[42]. For metabolomic measurements, snap frozen kidneys were cut to equal weights (20 mg per specimen) and mechanically homogenized into four volumes of ice-cold water. In brief, sugars, sugar phosphates, organic acids, bile acids, nucleotides and other anionic polar metabolites were measured in 30 μL of tissue homogenate using hydrophilic interaction liquid chromatography and multiple reaction monitoring in the negative ion mode on a 5500 QTRAP MS (SCIEX). Amino acids, amines, acylcarnitines, nucleotides, and other cationic polar metabolites were measured in 10 μl of tissue homogenate using hydrophilic interaction liquid chromatography coupled with nontargeted, positive ion mode MS analysis on an Exactive Plus Orbitrap MS (Thermo Scientific). Results were analysed in MetaboAnalyst (http://www.metaboanalyst.ca).

Statistics

Statistics were analyzed using Minitab express and GraphPad Prism. Any outliers in data were identified and excluded using GraphPad Prism. Comparisons between continuous characteristics of subject groups were analyzed with two-tailed Student's t-test using GraphPad Prism. For comparisons among more than two groups, one-way ANOVA with Tukey post hoc in Minitab express was used. Survival was analyzed by Kaplan-Meier estimation using GraphPad Prism. Overlap of S-nitrosylated proteins in three independent experiments (SNO-RAC-coupled quantitative MS) and interactions between the nitrosoproteome and SCoR/AKR1A1 interactome were analyzed using the SAS program. Sample size determination was guided by power calculations and prior experience. Mice were randomized to experimental intervention versus control. Each mouse was assigned a code number to enable blinded sham or AKI surgery. Samples were assigned a code number to enable blinded quantitative analyses and measurements including: metabolomics, iTRAQ-Coupled LC-MS/MS, SNO/FeNO (using photolysis/chemiluminescence), histology, mitochondrial morphology, serum creatinine and serum BUN. After all data were collected, the results were analyzed and decoded. Bar graphs with the corresponding dot plots were created using GraphPad Prism. Results are presented as mean ± SD.

Extended Data

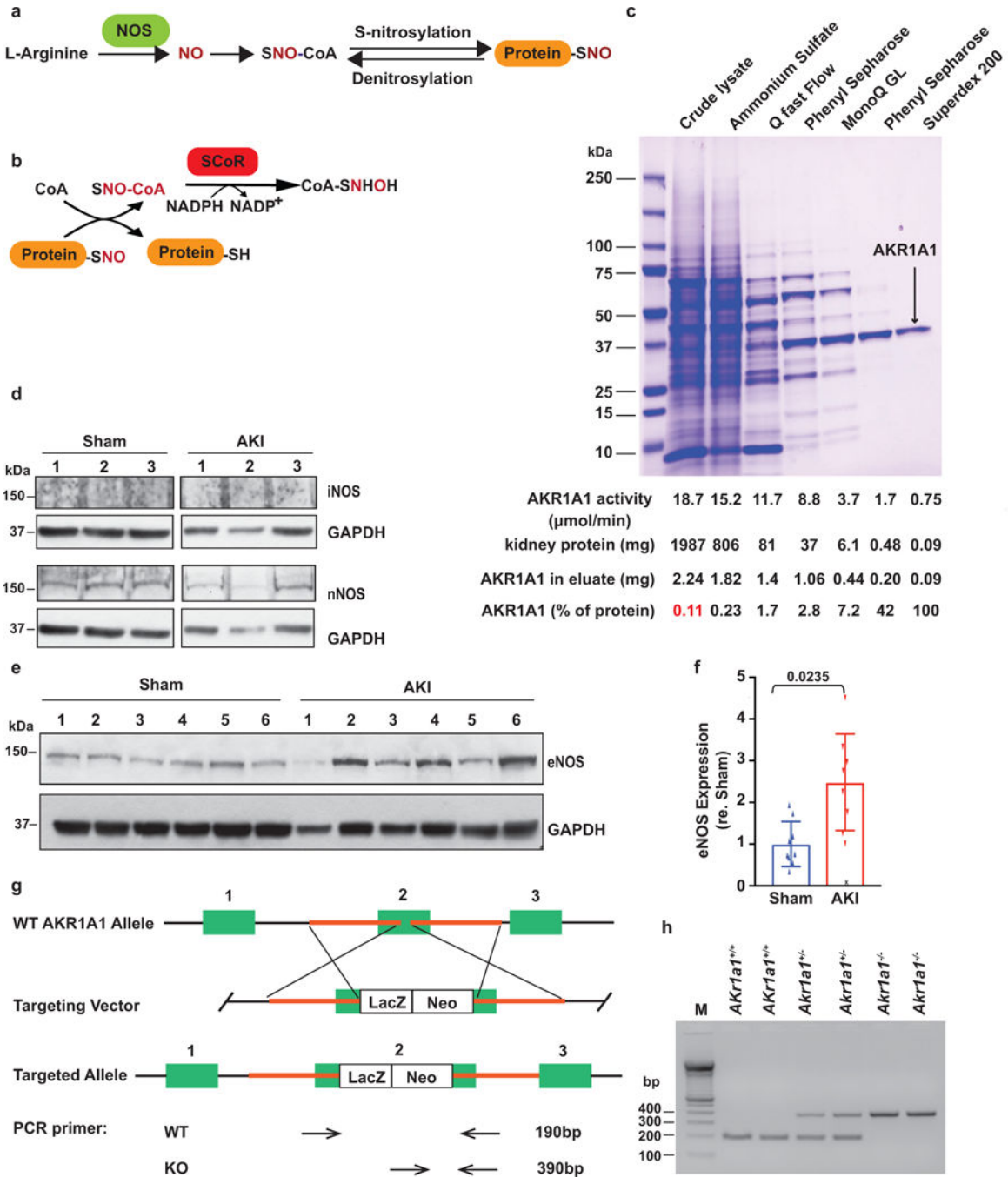

Extended Data Fig.1. Identification of enzymes involved in the SNO-CoA/SCoR system

(a-b) Enzymatic mechanism by which the SNO-CoA/SCoR system regulates protein S-nitrosylation. (a) Equilibrium between SNO-CoA and S-nitrosylated proteins. (b) AKR1A1 mediates protein denitrosylation. **(c)** AKR1A1 was purified to homogeneity using the indicated steps. AKR1A1 protein at each stage was calculated based on activity in each eluate pool or original crude lysate. Image is representative of two independently performed

experiments with similar results. **(d-e)** Expression of iNOS, nNOS and eNOS in sham-treated vs. injured kidneys of WT mice; injury induced by I/R. Images are representative of three independently performed experiments with similar results. For gel source data, see Supplementary Figure 1. **(f)** Expression of eNOS before and after AKI; normalized with GAPDH as in (d) (n=8 mice per group). Results are presented as mean ± SD. Two-tailed Student's t-test was used to detect significance. **(g)** Schema illustrating generation of *Akr1a1*$^{-/-}$ mice. **(h)** PCR amplification of the *Akr1a1* gene with genomic DNA isolated from the tails of *Akr1a1*$^{+/+}$ (WT), heterozygous *Akr1a1*$^{+/-}$ and homozygous *Akr1a1*$^{-/-}$ mice. Image is representative of three independently performed experiments with similar results..

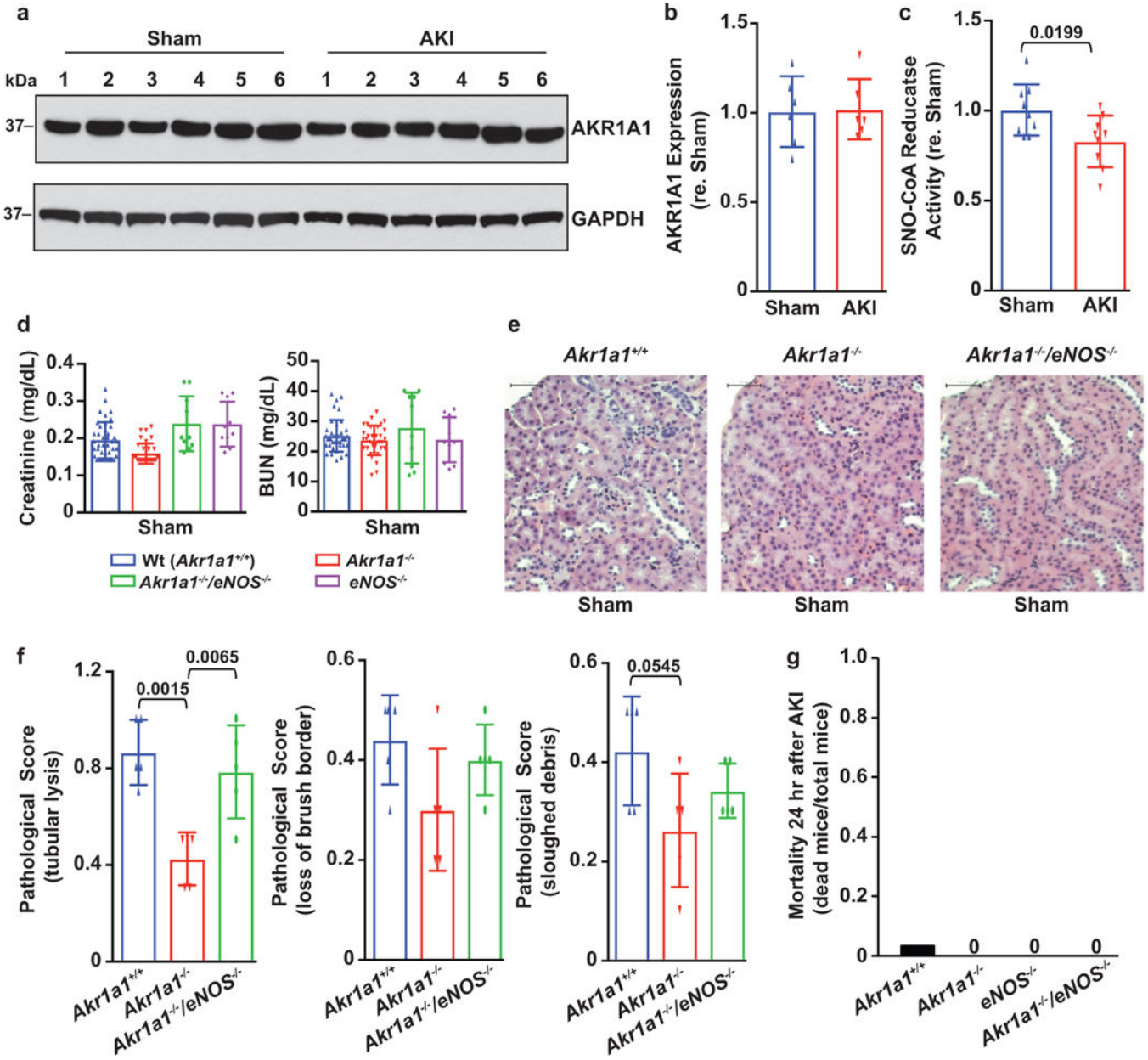

Extended Data Fig.2. SNO-CoA Reductase activity and role in protection

(a-b) Expression of AKR1A1 after I/R-induced AKI. Expression of AKR1A1 is normalized with GAPDH in (b) (n=6 mice per group). **(c)** NADPH-dependent SNO-CoA metabolizing activity measured in kidney extracts from sham-treated or WT mice subjected to I/R-induced AKI (n=9 mice per group). Two-tailed Student's t-test was used to detect significance. **(d)** Serum creatinine and blood urea nitrogen (BUN) in sham-treated kidneys of $Akr1a1^{+/+}$, $Akr1a1^{-/-}$, $Akr1a1^{-/-}/eNOS^{-/-}$ and $eNOS^{-/-}$ mice ($Akr1a1^{+/+}$: n=41 mice; $Akr1a1^{-/-}$: n=35 mice; $Akr1a1^{-/-}/eNOS^{-/-}$: n=10 mice; $eNOS^{-/-}$: n=10 mice). Note lower scales (y-axis) compared to Fig 1e-f. **(e)** H&E stain of sham-treated kidneys of $Akr1a1^{+/+}$, $Akr1a1^{-/-}$ and $Akr1a1^{-/-}/eNOS^{-/-}$ mice. Images are representative of two independently performed experiments with similar results. Scale bars, 50μm. **(f)** Pathological scores of tubular lysis, loss of brush border and sloughed debris (n=5 mice per group). Results are presented as mean ± SD. One-way ANOVA with Tukey post hoc was used to detect significance. **(g)** Mortality of $Akr1a1^{+/+}$, $Akr1a1^{-/-}$, $Akr1a1^{-/-}/eNOS^{-/-}$ and $eNOS^{-/-}$ mice 24 hours after AKI. ($Akr1a1^{+/+}$: 35 mice; $Akr1a1^{-/-}$: 36 mice; $Akr1a1^{-/-}/eNOS^{-/-}$: 12 mice; $eNOS^{-/-}$: 9 mice). Results are presented as mean ± SD. One-way ANOVA with Tukey post hoc was used to detect significance in Extended Data Fig.2d&f. Two-tailed Student's t-test was used to detect significance in Extended Data Fig.2b&c.

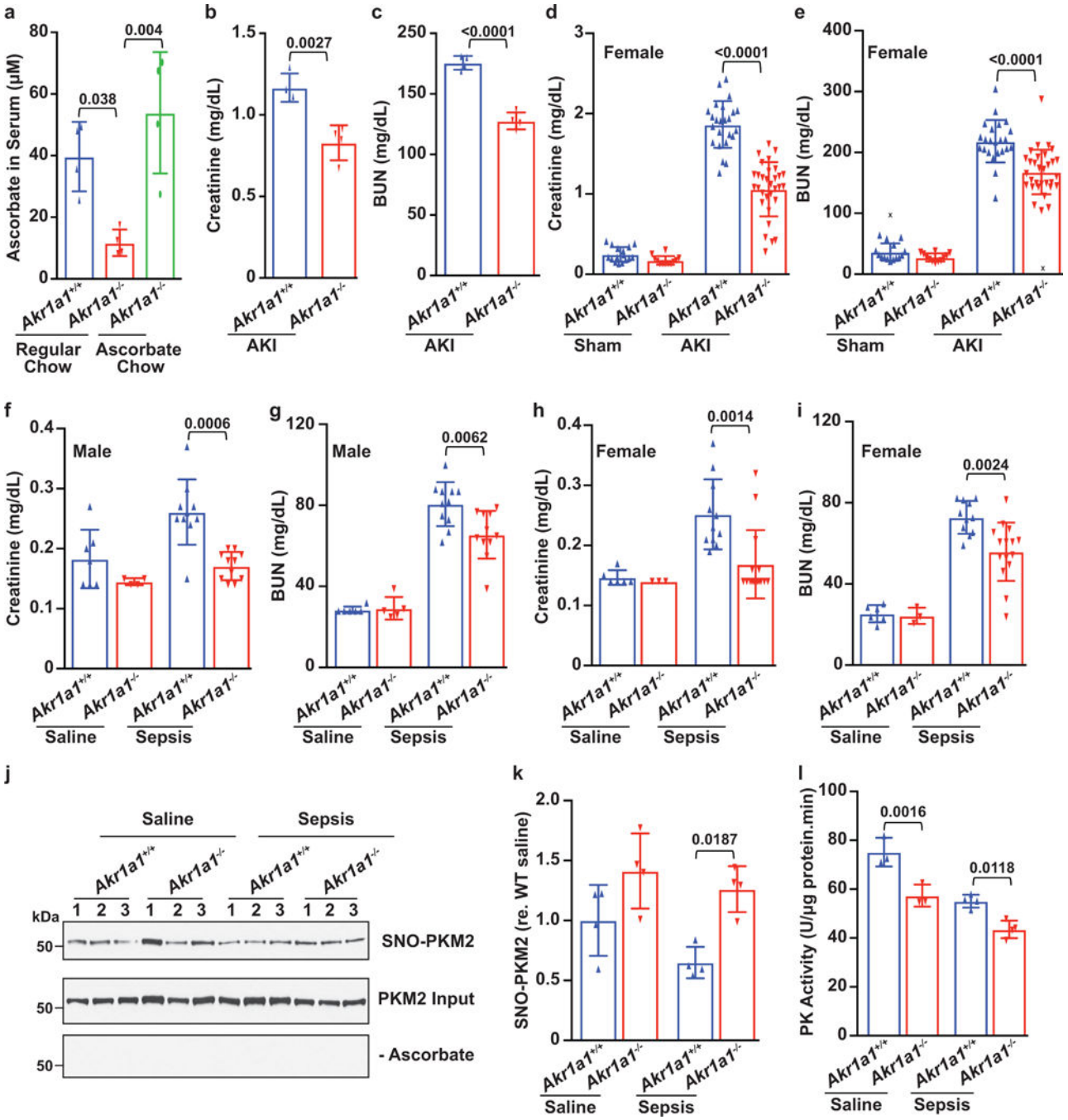

Extended Data Fig.3. Additional models of AKI

(a) Serum ascorbate in *Akr1a1*$^{+/+}$ vs. *Akr1a1*$^{-/-}$ mice fed with chow containing 1% ascorbic acid for six weeks (n=4 mice per group). **(b-c)** Serum creatinine and BUN in injured kidneys of *Akr1a1*$^{+/+}$ vs. *Akr1a1*$^{-/-}$ mice fed with chow containing 1% ascorbic acid for six weeks (n=4 mice per group); injury by I/R. **(d-e)** Serum creatinine and BUN in sham-treated or injured kidneys of female *Akr1a1*$^{+/+}$ vs. female *Akr1a1*$^{-/-}$ mice (sham-treated *Akr1a1*$^{+/+}$: n=11 mice; sham-treated *Akr1a1*$^{-/-}$: n=12 mice; injured *Akr1a1*$^{+/+}$: n=25 mice; injured *Akr1a1*$^{-/-}$: n=31 mice). Injury by I/R. **(f-g)** Serum creatinine and BUN in saline-treated or

LPS-treated male *Akr1a1*$^{+/+}$ vs. *Akr1a1*$^{-/-}$ mice (saline-treated *Akr1a1*$^{+/+}$: n=7 mice; saline-treated *Akr1a1*$^{-/-}$: n=5 mice; LPS-treated *Akr1a1*$^{+/+}$: n=11 mice; LPS-treated *Akr1a1*$^{-/-}$: n=11 mice). **(h-i)** Serum creatinine and BUN in saline-treated or LPS-treated female *Akr1a1*$^{+/+}$ vs. *Akr1a1*$^{-/-}$ mice (saline-treated *Akr1a1*$^{+/+}$: n=6 mice; saline-treated *Akr1a1*$^{-/-}$: n=3 mice; LPS-treated *Akr1a1*$^{+/+}$: n=12 mice; LPS-treated *Akr1a1*$^{-/-}$: n=15 mice). **(j)** Endogenous S-nitrosylation of PKM2 in saline-treated or LPS-treated male *Akr1a1*$^{+/+}$ and *Akr1a1*$^{-/-}$ mice. Data are representative of three mice per genotype. Without ascorbate (-Ascorbate) is control for SNO. **(k)** Quantification of SNO-PKM2. SNO is normalized to PKM2 (input)(n=4 mice per group). **(l)** Activity of endogenous pyruvate kinase in saline- or LPS-treated kidneys of *Akr1a1*$^{+/+}$ and *Akr1a1*$^{-/-}$ mice (n=3 mice per saline-treated group; n=5 mice per LPS-treated group). Results are presented as mean ± SD. One-way ANOVA with Tukey post hoc was used to detect significance in Extended Data Fig.3a and 3d-l. Two-tailed Student's t-test was used to detect significance in Extended Data Fig.3b&c.

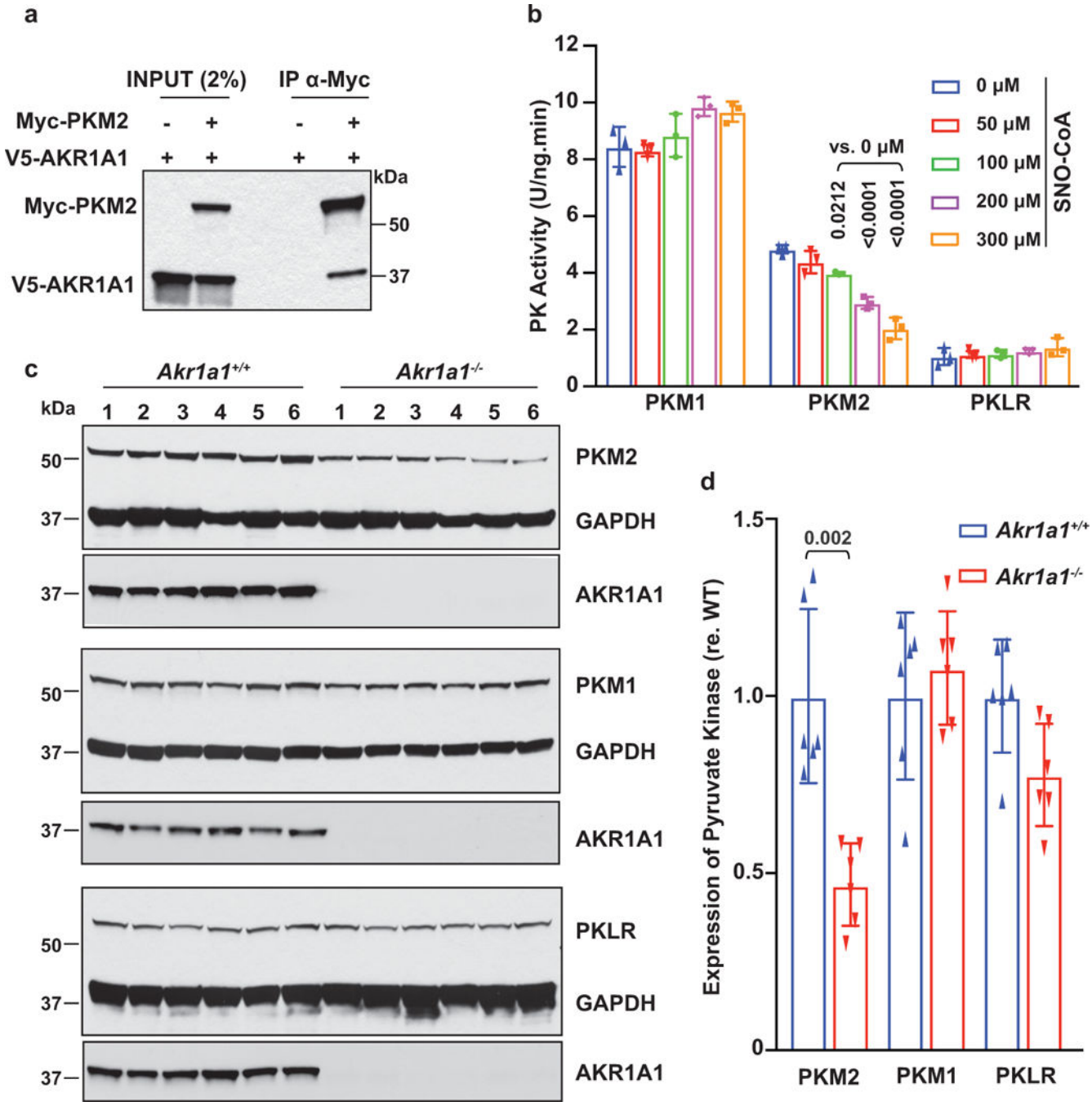

Extended Data Fig.4. PK interactions, activity and expression

(a) Interaction between AKR1A1 and PKM2. Myc-PKM2 and V5-AKR1A1 are co-overexpressed in HEK cells. IP with anti-Myc rabbit antibody; IB with V5 antibody. Image is representative of two independently performed experiments with similar results. **(b)** Activity of recombinant PKM2, PKM1 and PKLR proteins after SNO-CoA treatment (n=3 independent experiments). Results are presented as mean ± SD. One-way ANOVA with Tukey post hoc was used to assess significance. **(c)** Expression of PKM2, PKM1 and PKLR in the kidney of *Akr1a1*$^{+/+}$ and *Akr1a1*$^{-/-}$ mice after 24- hours of I/R-induced AKI. Image is

representative of two independently performed experiments with similar results. **(d)** Quantification of expression of PKM2, PKM1 and PKLR in (c)(n=6 mice per group). Result is presented as mean ± SD. Two-tailed Student's t-test was used to detect significance.

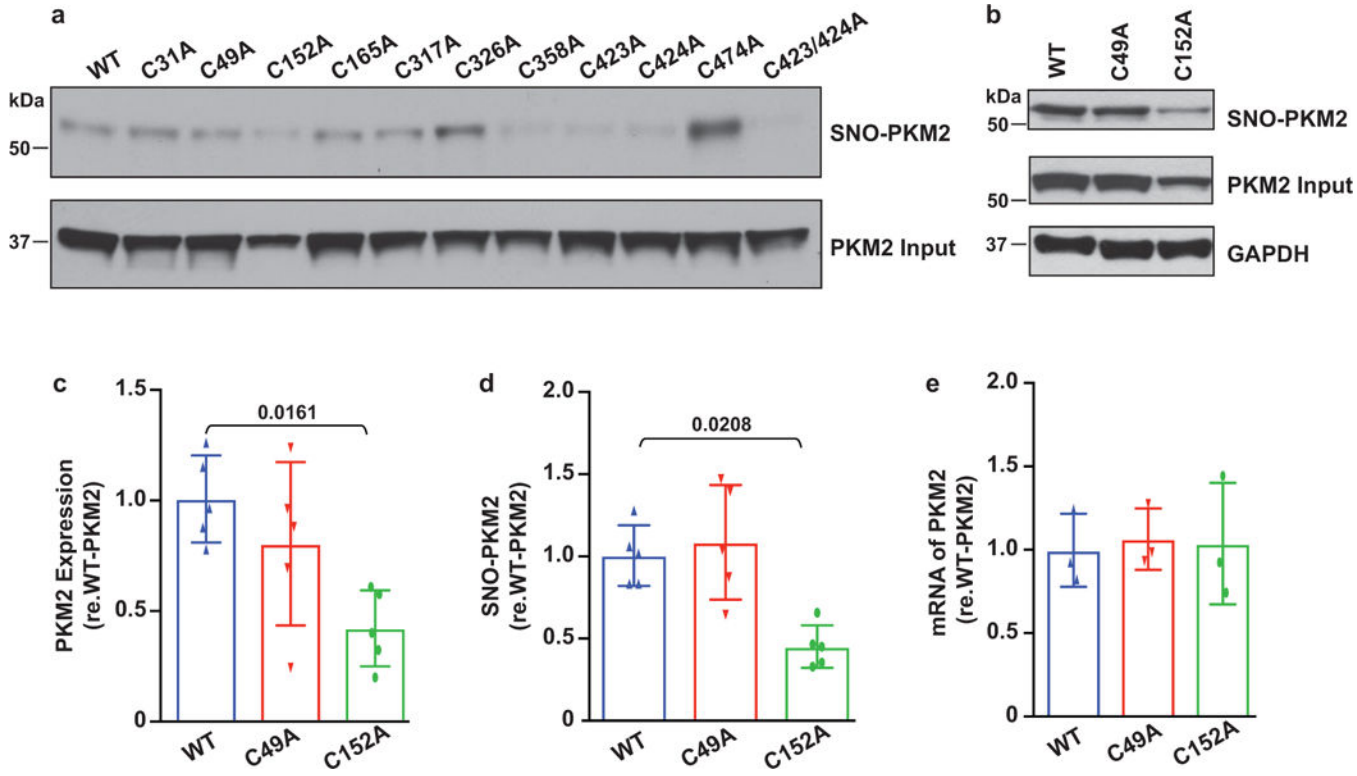

Extended Data Fig.5. Characterization of SNO-PKM2

(a) Endogenous SNO level of PKM2 Cys-mutants in eNOS-overexpressing HEK cells. Image is representative of two independently performed experiments with similar results. **(b)** Mutation of C152 to alanine affects the SNO level of PKM2 in eNOS-overexpressing HEK cells. Image is representative of two independently performed experiments with similar results. **(c)** Quantification of expression of Myc-PKM2-wild-type (WT), Myc-PKM2-C49A and Myc-PKM2-C152A in eNOS-overexpressing HEK cells. Normalized with expression of GAPDH (n=5 independent experiments). **(d)** Quantification of SNO-PKM2 in eNOS-overexpressing HEK cells. SNO is normalized to PKM2 (input) (n=5 independent experiments). **(e)** Relative mRNA level of Myc-PKM2-WT, Myc-PKM2-C49A and Myc-PKM2-C152A in eNOS-overexpressing HEK cells (n=3 independent experiments). Results in Extended Data Fig.5c-e are presented as mean ± SD. One-way ANOVA with Tukey post hoc was used to detect significance...

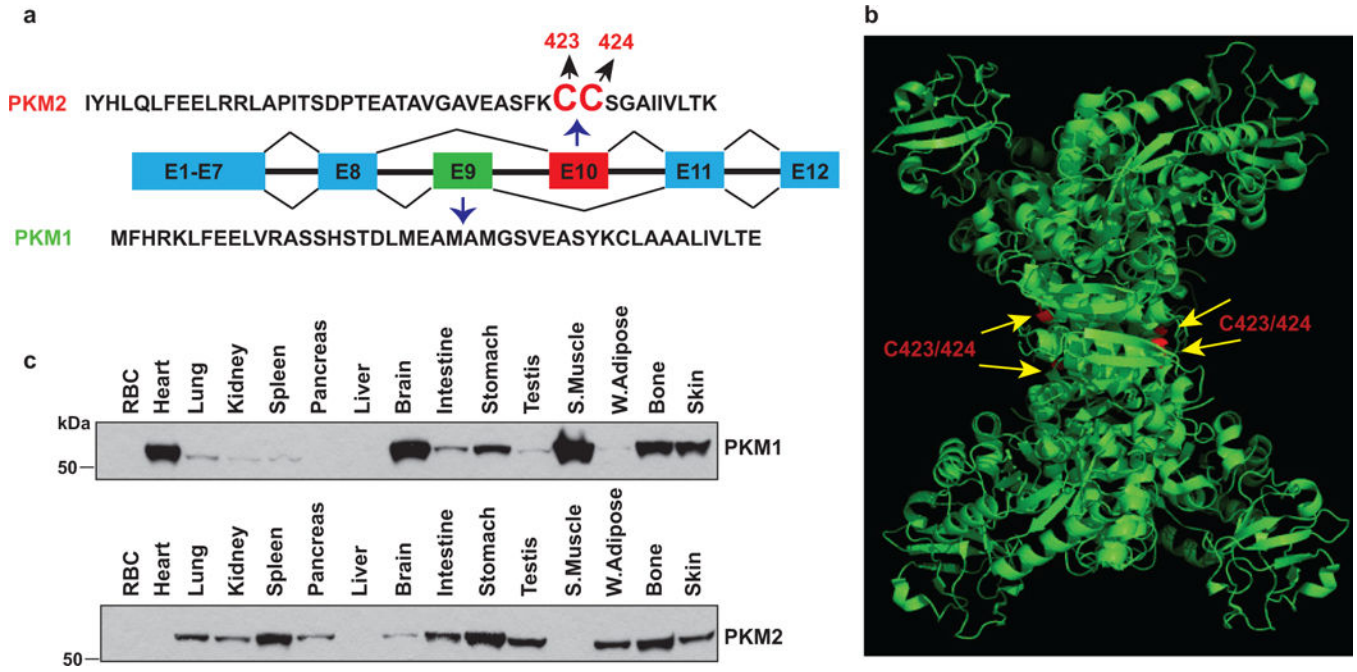

Extended Data Fig.6. PKM gene, structure and expression

(a) Alternative splicing of PKM gene. C423 and C424 are encoded by PKM2-specific exon 10. **(b)** Ribbon structure of tetrameric PKM2 analyzed by MacPyMOL. Four pairs of C423 and C424 in tetrameric PKM2 are highlighted in red. **(c)** Expression of PKM1 and PKM2 in fifteen different tissues from uninjured mice. Image is representative of two independently performed experiments with similar results.

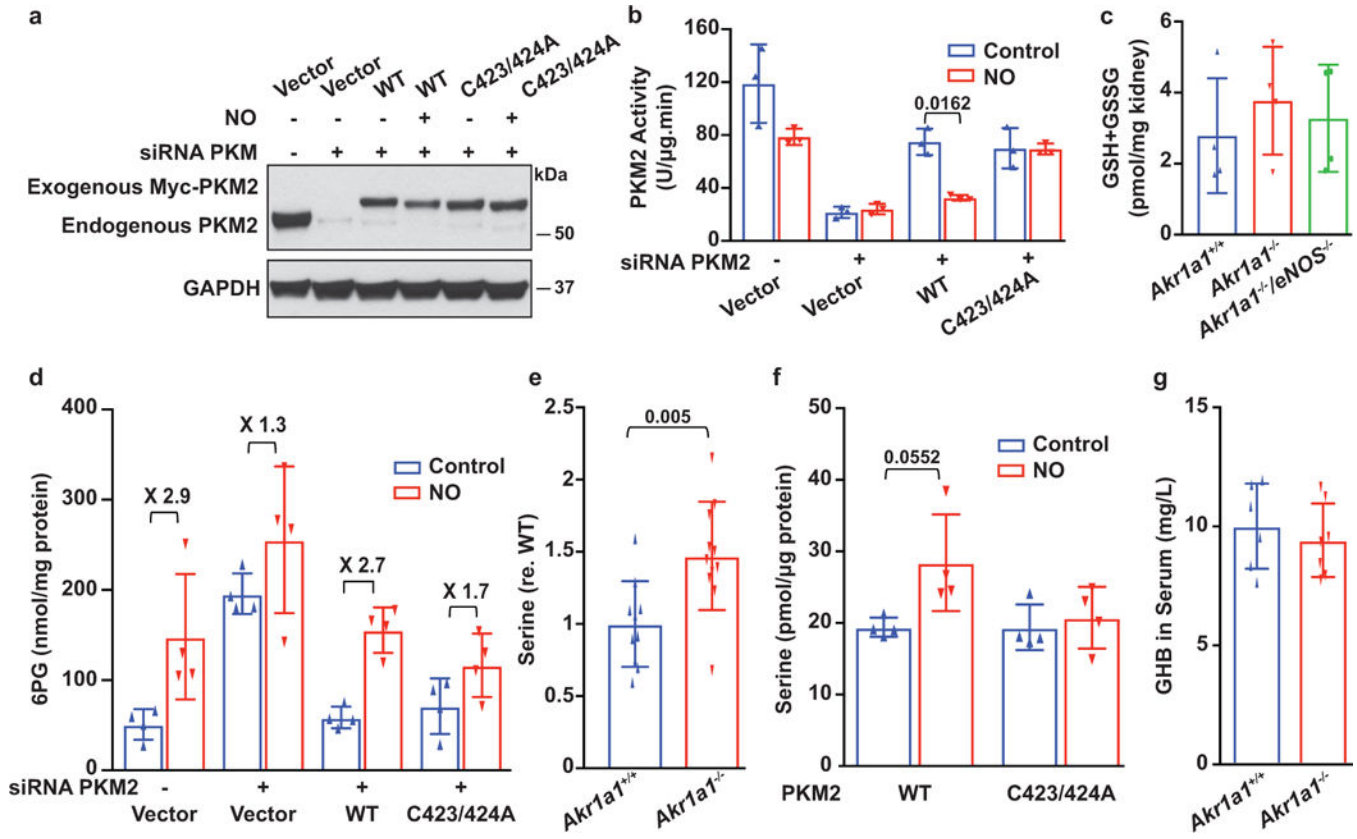

Extended Data Fig.7. Role of PKM2 in AKR1A1-mediated protection

(a) Expression of endogenous and overexpressed PKM2 in HEK cells. Image is representative of two independently performed experiments with similar results. **(b)** Activity of Myc-PKM2-WT and Myc-PKM2-C423/424A after NO (DETANO; 500µM) treatment in HEK cells (n=3 independent experiments). **(c)** The total amount of GSH+GSSG in injured kidneys of *Akr1a1*$^{+/+}$, *Akr1a1*$^{-/-}$ and *Akr1a1*$^{-/-}$/*eNOS*$^{-/-}$ mice (n=4 mice per group); injury induced by I/R. **(d)** The amount of 6-phosphogluconate (6PG), a key PPP intermediate, in Myc-PKM2-WT and Myc-PKM2 C423/424A expressing HEK cells after NO (DETANO; 500µM) treatment (n=4 independent experiments). **(e)** Amount of serine in injured kidneys of *Akr1a1*$^{+/+}$ vs. *Akr1a1*$^{-/-}$ mice (n=10 mice per sham-treated *Akr1a1*$^{+/+}$ or I/R-injured *Akr1a1*$^{+/+}$ group; n=11 mice per sham-treated *Akr1a1*$^{-/-}$ or I/R-injured *Akr1a1*$^{-/-}$group); injury induced by I/R. **(f)** Amount of serine in Myc-PKM2-WT and Myc-PKM2-C423/424A HEK cells after NO treatment (DETANO; 500µM) (n=4 independent experiments). **(g)** Amount of gamma-hydroxybutyric acid (GHB) in serum of *Akr1a1*$^{+/+}$ vs. *Akr1a1*$^{-/-}$ mice (n= 7 mice per group). No injury.

Results are presented as mean ± SD. One-way ANOVA with Tukey post hoc was used to detect significance.

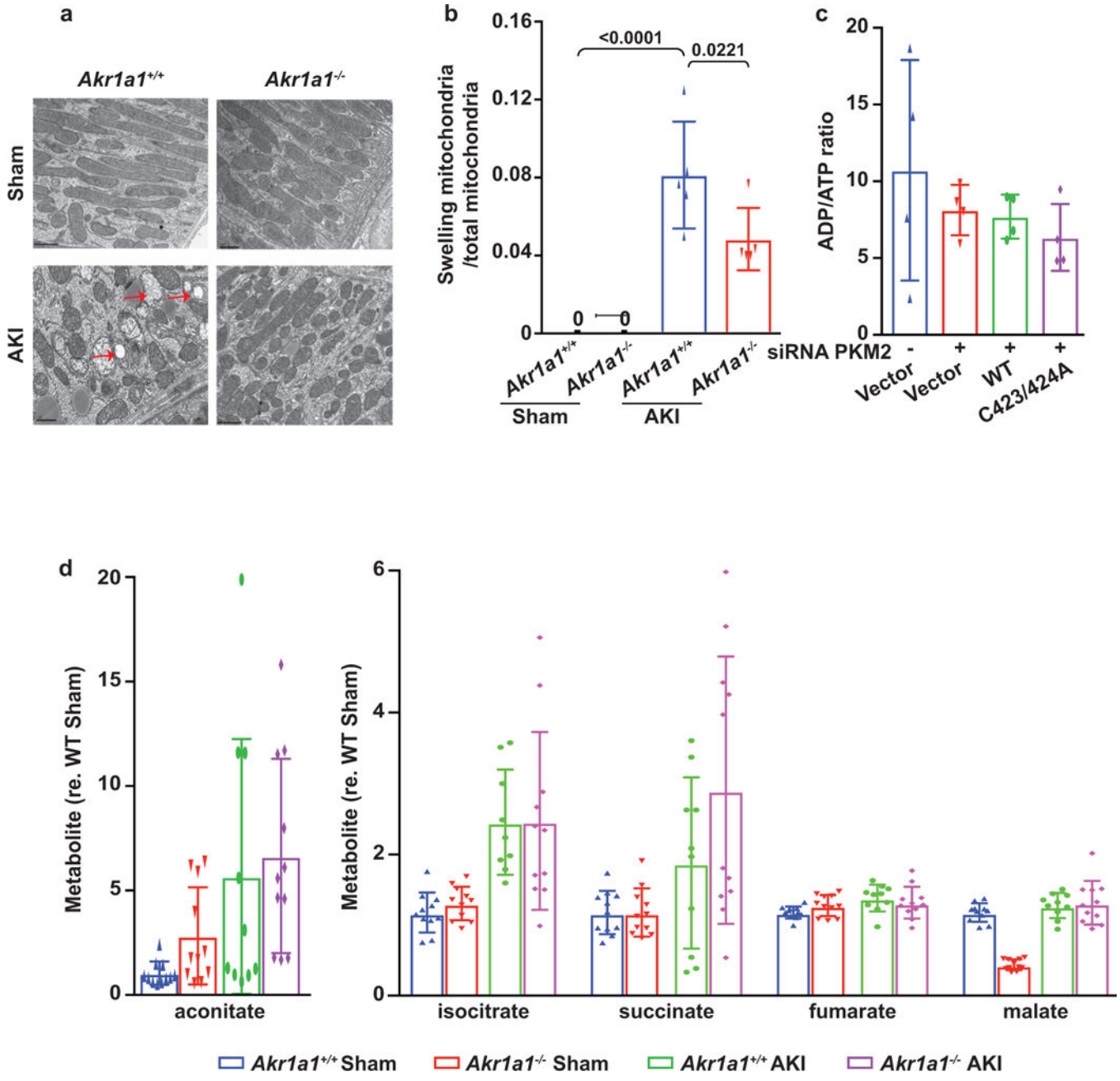

Extended Data Fig.8. Mechanism of kidney injury

(a) Mitochondrial morphology in tubule cells after sham operation or injury induced by I/R from *Akr1a1*$^{+/+}$ vs. *Akr1a1*$^{-/-}$ mice as assessed by electron microscopy. Mitochondrial swelling is indicated by the red arrows. Scale bars, 1μm. **(b)** Quantification of swollen mitochondria vs. total mitochondria in sham-treated or I/R-injured kidneys from *Akr1a1*$^{+/+}$ vs. *Akr1a1*$^{-/-}$ mice. Two-tailed Student's t-test was used to detect significance. Results are presented as mean ± SD. One-way ANOVA with Tukey post hoc was used to detect significance. **(c)** The ratio of ADP vs. ATP in Myc-PKM2-WT and Myc-PKM2-C423/424A HEK cells after NO (DETANO; 500μM) (n=4 independent experiments). **(d)** Amounts of TCA cycle intermediates (aconitate, isocitrate, succinate, fumarate and malate) in sham-

treated or injured kidneys of *Akr1a1*$^{+/+}$ vs. *Akr1a1*$^{-/-}$ mice (n=10 mice per sham-treated *Akr1a1*$^{+/+}$ or I/R-injured *Akr1a1*$^{+/+}$ group; n=11 mice per sham-treated *Akr1a1*$^{-/-}$ or I/R-injured *Akr1a1*$^{-/-}$group); injury induced with I/R. Results are presented as mean ± SD. There are no significant differences in Extended Data Fig.8c&d using one-way ANOVA with Tukey post hoc..

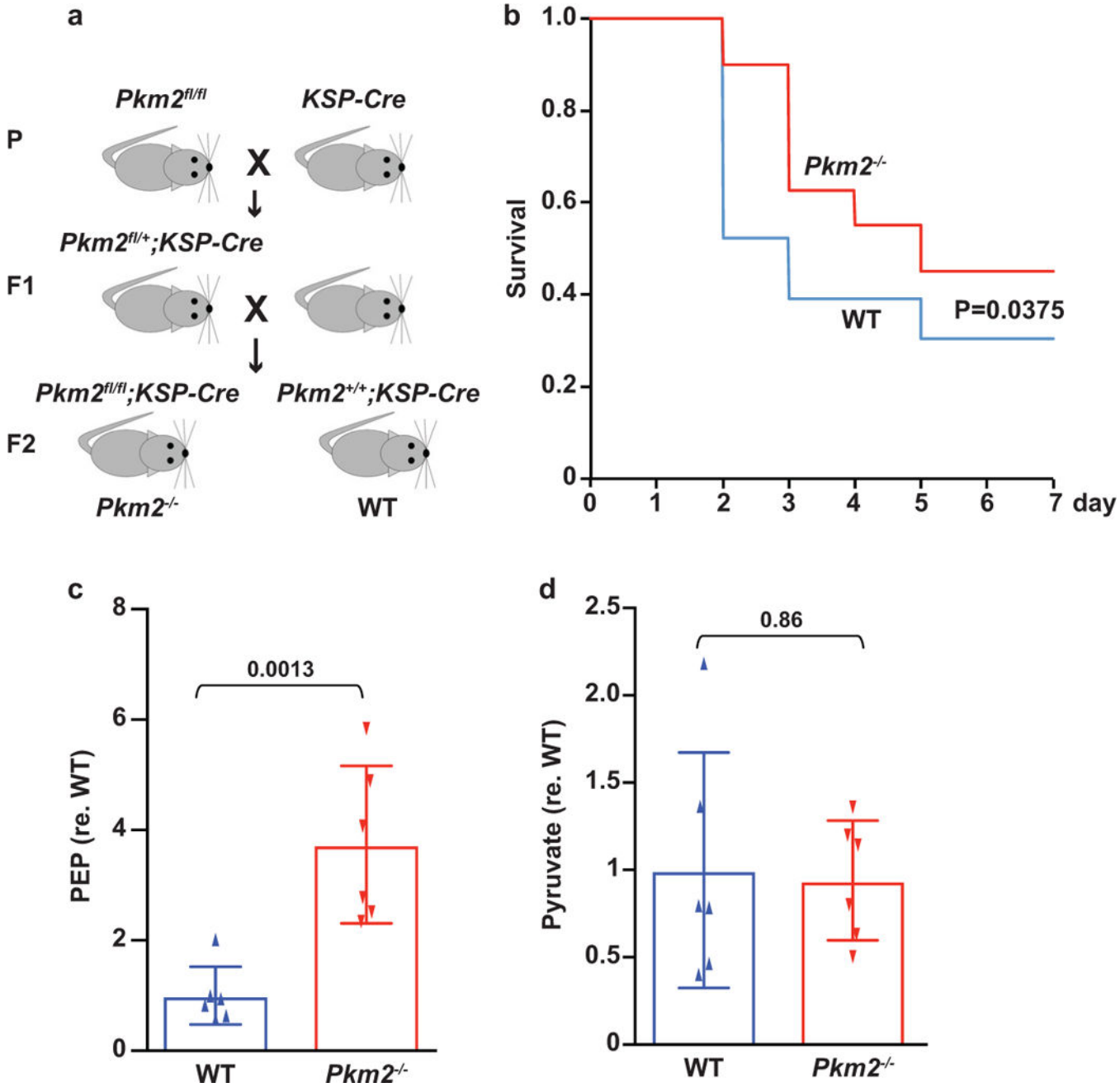

Extended Data Fig.9. Characterization of *Pkm2*$^{-/-}$ mice

(a) Schema illustrating generation of renal epithelial cell-specific *Pkm2*$^{-/-}$ mice. **(b)** Survival curve following I/R-induced AKI (23 WT mice; 20 *Pkm2*$^{-/-}$ mice). Survival was

analyzed using Kaplan-Meier estimation. Gehan–Breslow–Wilcoxon test, P=0.0375. **(c)** Phosphoenolpyruvate (PEP) in injured kidneys of WT vs. *Pkm2*$^{-/-}$ mice (n=6 mice per group); injury induced by I/R. **(d)** Pyruvate in injured kidneys of WT vs. *Pkm2*$^{-/-}$ mice (n=6 mice per group). Results in Extended Data Fig.9c&d are presented as mean ± SD. Two-tailed Student's t-test was used to detect significance.

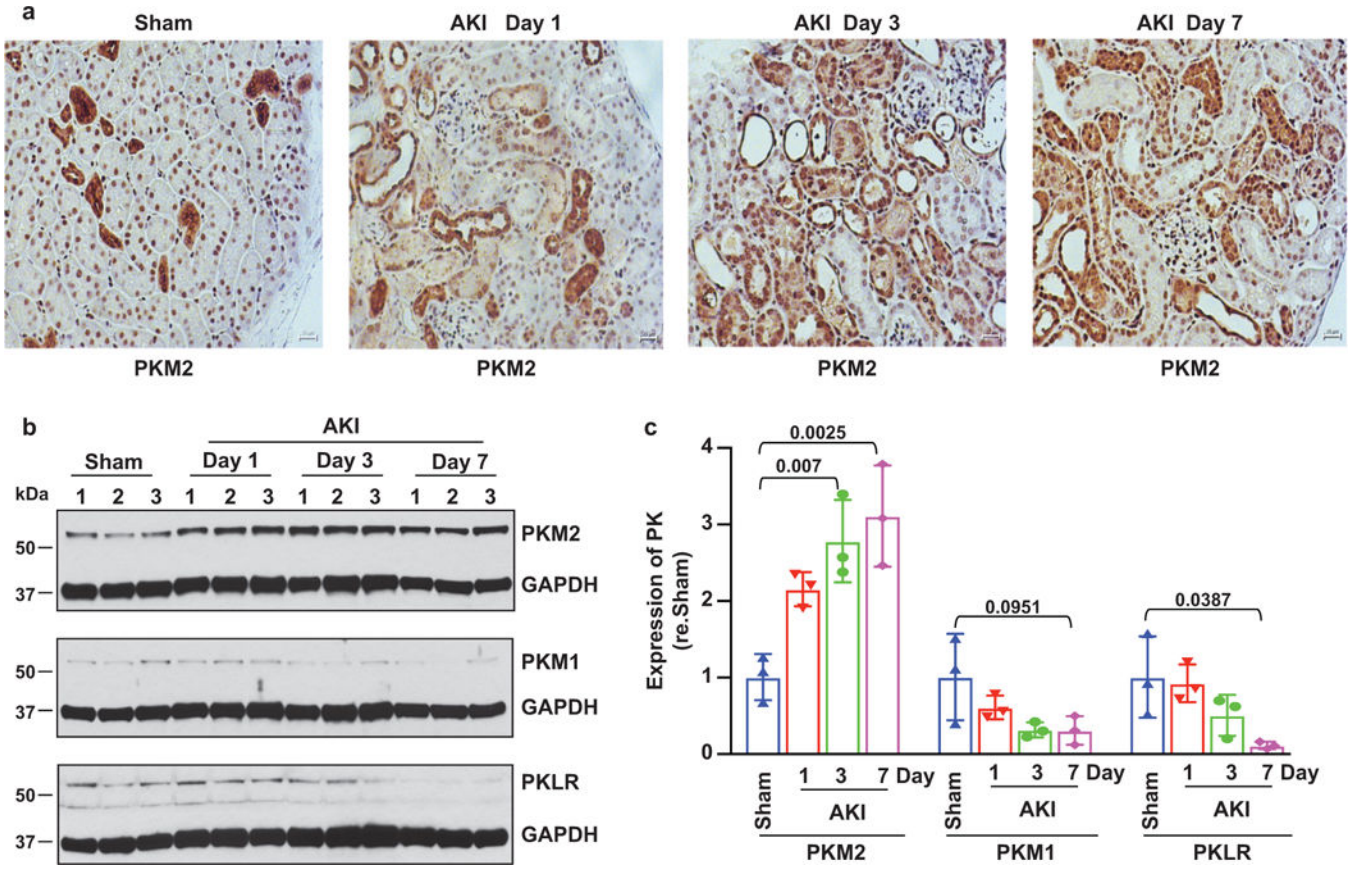

Extended Data Fig.10. Expression of PKM1, PKM2 and PKLR after AKI

(a) Immunostaining showing expression of PKM2 in sham or injured kidneys of WT mice on the indicated days after surgery; injury induced by I/R. Images are representative of two independently performed experiments with similar results. **(b)** Western blot showing expression of PKM2, PKM1 and PKLR in sham or injured kidneys of WT mice; injury induced by I/R. Images are representative of two independently performed experiments similar results. **(c)** Quantification of expression of PKM2, PKM1 and PKLR in (b) (n=3 mice). Results are presented as mean ± SD. One-way ANOVA with Tukey post hoc was used to detect significance.

Supplementary Material

Refer to Web version on PubMed Central for supplementary material.

Acknowledgements

We thank H. Fujioka from the Electron Microscopy Core Facility of CWRU for mitochondrial analyses, J. Mikulan and A. Kresak from the Tissue Resources Core of CWRU for histology and immunostaining, and Cuiyu Geng from the Cleveland Clinic Foundation for assistance with statistics. We thank J. Reynolds, D. Hess, R. Premont and D. Seth for discussions. This work is supported by National Institutes of Health grants DK119506, HL075443, HL128192 and HL126900.

References

1. Wang W et al. Endothelial nitric oxide synthase-deficient mice exhibit increased susceptibility to endotoxin-induced acute renal failure. Am J Physiol Renal Physiol 287, F1044–1048, doi:10.1152/ajprenal.00136.2004 (2004). [PubMed: 15475535]
2. Forbes MS, Thornhill BA, Park MH & Chevalier RL Lack of endothelial nitric-oxide synthase leads to progressive focal renal injury. Am J Pathol 170, 87–99, doi:10.2353/ajpath.2007.060610 (2007). [PubMed: 17200185]
3. Seth D et al. A Multiplex Enzymatic Machinery for Cellular Protein S-nitrosylation. Mol Cell 69, 451–464 e456, doi:10.1016/j.molcel.2017.12.025 (2018). [PubMed: 29358078]
4. Stomberski CT, Hess DT & Stamler JS Protein S-Nitrosylation: Determinants of Specificity and Enzymatic Regulation of S-Nitrosothiol-Based Signaling. Antioxid Redox Signal, doi:10.1089/ars.2017.7403 (2018).
5. Anand P et al. Identification of S-nitroso-CoA reductases that regulate protein S-nitrosylation. Proc Natl Acad Sci U S A 111, 18572–18577, doi:10.1073/pnas.1417816112 (2014). [PubMed: 25512491]
6. Nagasu H et al. Endothelial dysfunction promotes the transition from compensatory renal hypertrophy to kidney injury after unilateral nephrectomy in mice. Am J Physiol Renal Physiol 302, F1402–1408, doi:10.1152/ajprenal.00459.2011 (2012). [PubMed: 22378818]
7. Gabbay KH et al. Ascorbate synthesis pathway: dual role of ascorbate in bone homeostasis. J Biol Chem 285, 19510–19520, doi:10.1074/jbc.M110.110247 (2010). [PubMed: 20410296]
8. Jia J et al. Target-selective protein S-nitrosylation by sequence motif recognition. Cell 159, 623–634, doi:10.1016/j.cell.2014.09.032 (2014). [PubMed: 25417112]
9. Lan R et al. Mitochondrial Pathology and Glycolytic Shift during Proximal Tubule Atrophy after Ischemic AKI. J Am Soc Nephrol 27, 3356–3367, doi:10.1681/ASN.2015020177 (2016). [PubMed: 27000065]
10. Kang HM et al. Defective fatty acid oxidation in renal tubular epithelial cells has a key role in kidney fibrosis development. Nat Med 21, 37–46, doi:10.1038/nm.3762 (2015). [PubMed: 25419705]
11. Chang GG & Tong L Structure and function of malic enzymes, a new class of oxidative decarboxylases. Biochemistry 42, 12721–12733, doi:10.1021/bi035251+ (2003). [PubMed: 14596586]
12. Gray LR, Tompkins SC & Taylor EB Regulation of pyruvate metabolism and human disease. Cell Mol Life Sci 71, 2577–2604, doi:10.1007/s00018-013-1539-2 (2014). [PubMed: 24363178]
13. Anastasiou D et al. Inhibition of pyruvate kinase M2 by reactive oxygen species contributes to cellular antioxidant responses. Science 334, 1278–1283, doi:10.1126/science.1211485 (2011). [PubMed: 22052977]
14. Qi W et al. Pyruvate kinase M2 activation may protect against the progression of diabetic glomerular pathology and mitochondrial dysfunction. Nat Med 23, 753–762, doi:10.1038/nm.4328 (2017). [PubMed: 28436957]
15. Fan J et al. Quantitative flux analysis reveals folate-dependent NADPH production. Nature 510, 298–302, doi:10.1038/nature13236 (2014). [PubMed: 24805240]
16. Kim J et al. Role of cytosolic NADP+-dependent isocitrate dehydrogenase in ischemia-reperfusion injury in mouse kidney. Am J Physiol Renal Physiol 296, F622–633, doi:10.1152/ajprenal.90566.2008 (2009). [PubMed: 19106211]

17. Sharfuddin AA & Molitoris BA Pathophysiology of ischemic acute kidney injury. Nat Rev Nephrol 7, 189–200, doi:10.1038/nrneph.2011.16 (2011). [PubMed: 21364518]
18. Granger DN & Kvietys PR Reperfusion injury and reactive oxygen species: The evolution of a concept. Redox Biol 6, 524–551, doi:10.1016/j.redox.2015.08.020 (2015). [PubMed: 26484802]
19. Zuk A & Bonventre JV Acute Kidney Injury. Annu Rev Med 67, 293–307, doi:10.1146/annurev-med-050214-013407 (2016). [PubMed: 26768243]
20. Ratliff BB, Abdulmahdi W, Pawar R & Wolin MS Oxidant Mechanisms in Renal Injury and Disease. Antioxid Redox Signal 25, 119–146, doi:10.1089/ars.2016.6665 (2016). [PubMed: 26906267]
21. Benavides GA, Liang Q, Dodson M, Darley-Usmar V & Zhang J Inhibition of autophagy and glycolysis by nitric oxide during hypoxia-reoxygenation impairs cellular bioenergetics and promotes cell death in primary neurons. Free Radic Biol Med 65, 1215–1228, doi:10.1016/j.freeradbiomed.2013.09.006 (2013). [PubMed: 24056030]
22. Almeida A, Moncada S & Bolanos JP Nitric oxide switches on glycolysis through the AMP protein kinase and 6-phosphofructo-2-kinase pathway. Nat Cell Biol 6, 45–51, doi:10.1038/ncb1080 (2004). [PubMed: 14688792]
23. Bolanos JP, Delgado-Esteban M, Herrero-Mendez A, Fernandez-Fernandez S & Almeida A Regulation of glycolysis and pentose-phosphate pathway by nitric oxide: impact on neuronal survival. Biochim Biophys Acta 1777, 789–793, doi:10.1016/j.bbabio.2008.04.011 (2008). [PubMed: 18455501]
24. O'Connor T, Ireland LS, Harrison DJ & Hayes JD Major differences exist in the function and tissue-specific expression of human aflatoxin B1 aldehyde reductase and the principal human aldo-keto reductase AKR1 family members. Biochem J 343 Pt 2, 487–504 (1999). [PubMed: 10510318]
25. Alzeer S & Ellis EM The role of aldehyde reductase AKR1A1 in the metabolism of gamma-hydroxybutyrate in 1321N1 human astrocytoma cells. Chem Biol Interact 191, 303–307, doi:10.1016/j.cbi.2011.01.018 (2011). [PubMed: 21276435]
26. Barski OA, Tipparaju SM & Bhatnagar A The aldo-keto reductase superfamily and its role in drug metabolism and detoxification. Drug Metab Rev 40, 553–624, doi:10.1080/03602530802431439 (2008). [PubMed: 18949601]
27. Doulias PT, Tenopoulou M, Greene JL, Raju K & Ischiropoulos H Nitric oxide regulates mitochondrial fatty acid metabolism through reversible protein S-nitrosylation. Sci Signal 6, rs1, doi:10.1126/scisignal.2003252 (2013). [PubMed: 23281369]
28. Anastasiou D et al. Pyruvate kinase M2 activators promote tetramer formation and suppress tumorigenesis. Nat Chem Biol 8, 839–847, doi:10.1038/nchembio.1060 (2012). [PubMed: 22922757]
29. Christofk HR et al. The M2 splice isoform of pyruvate kinase is important for cancer metabolism and tumour growth. Nature 452, 230–233, doi:10.1038/nature06734 (2008). [PubMed: 18337823]
30. Ye J et al. Pyruvate kinase M2 promotes de novo serine synthesis to sustain mTORC1 activity and cell proliferation. Proc Natl Acad Sci U S A 109, 6904–6909, doi:10.1073/pnas.1204176109 (2012). [PubMed: 22509023]

Additional References

31. Israelsen WJ et al. PKM2 isoform-specific deletion reveals a differential requirement for pyruvate kinase in tumor cells. Cell 155, 397–409, doi:10.1016/j.cell.2013.09.025 (2013). [PubMed: 24120138]
32. Shao X, Somlo S & Igarashi P Epithelial-specific Cre/lox recombination in the developing kidney and genitourinary tract. J Am Soc Nephrol 13, 1837–1846 (2002). [PubMed: 12089379]
33. Tran MT et al. PGC1alpha drives NAD biosynthesis linking oxidative metabolism to renal protection. Nature 531, 528–532, doi:10.1038/nature17184 (2016). [PubMed: 26982719]
34. Forrester MT et al. Proteomic analysis of S-nitrosylation and denitrosylation by resin-assisted capture. Nat Biotechnol 27, 557–559, doi:10.1038/nbt.1545 (2009). [PubMed: 19483679]

35. Zhou HL, Geng C, Luo G & Lou H The p97-UBXD8 complex destabilizes mRNA by promoting release of ubiquitinated HuR from mRNP. Genes Dev 27, 1046–1058, doi:10.1101/gad.215681.113 (2013). [PubMed: 23618873]

36. Stamler JS et al. Nitric oxide circulates in mammalian plasma primarily as an S-nitroso adduct of serum albumin. Proc Natl Acad Sci U S A 89, 7674–7677 (1992). [PubMed: 1502182]

37. Solez K, Morel-Maroger L & Sraer JD The morphology of “acute tubular necrosis” in man: analysis of 57 renal biopsies and a comparison with the glycerol model. Medicine (Baltimore) 58, 362–376 (1979). [PubMed: 481195]

38. Conger JD, Schultz MF, Miller F & Robinette JB Responses to hemorrhagic arterial pressure reduction in different ischemic renal failure models. Kidney Int 46, 318–323 (1994). [PubMed: 7967342]

39. Fujioka H, Tandler B & Hoppel CL Mitochondrial division in rat cardiomyocytes: an electron microscope study. Anat Rec (Hoboken) 295, 1455–1461, doi:10.1002/ar.22523 (2012). [PubMed: 22753088]

40. Hanaichi T et al. A stable lead by modification of Sato’s method. J Electron Microsc (Tokyo) 35, 304–306 (1986). [PubMed: 2440973]

41. Hitosugi T et al. Tyrosine phosphorylation inhibits PKM2 to promote the Warburg effect and tumor growth. Sci Signal 2, ra73, doi:10.1126/scisignal.2000431 (2009). [PubMed: 19920251]

42. Paynter NP et al. Metabolic Predictors of Incident Coronary Heart Disease in Women. Circulation 137, 841–853, doi:10.1161/CIRCULATIONAHA.117.029468 (2018). [PubMed: 29459470]

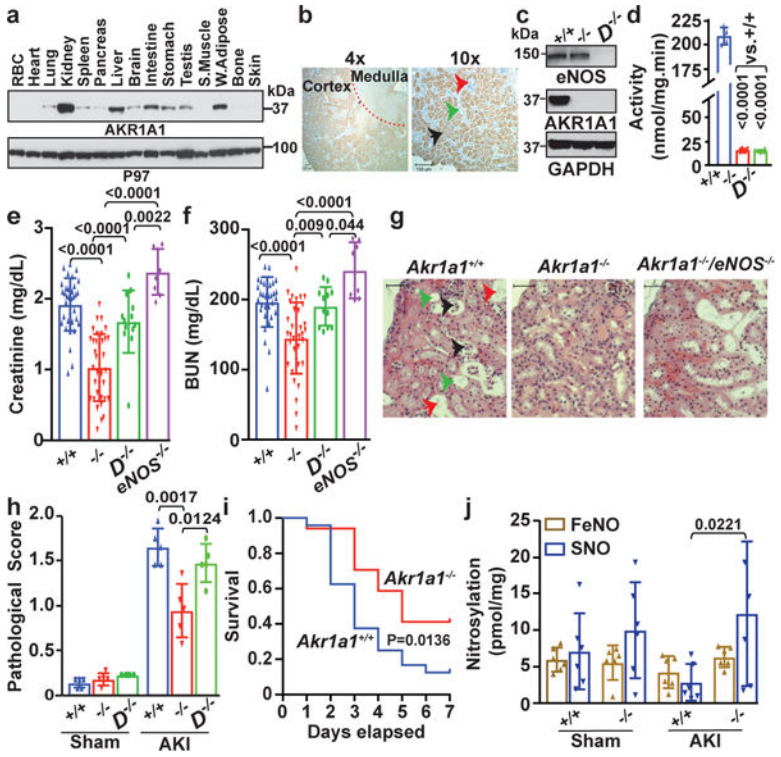

Figure 1. Knockout of AKR1A1 protects against AKI in a SNO-dependent manner.

(a) Expression of AKR1A1 in 15 different mouse tissues. AAA ATPase P97 is used as loading control. **(b)** Expression of AKR1A1 in proximal tubule. Immunostaining: 10x image derives from cortex area in 4x image. Proximal tubule (black arrow); Distal tubule (green arrow); Glomerulus (red arrow). Scale bars in both 4x image and 10x image,100μm. **(c)** Expression of AKR1A1 and eNOS in the kidneys of wild-type control (*Akr1a1*$^{+/+}$)($^{+/+}$), *Akr1a1*$^{-/-}$ ($^{-/-}$) and *Akr1a1*$^{-/-}$/*eNOS*$^{-/-}$ (D$^{-/-}$) mice. **(d)** NADPH-dependent SNO-CoA metabolizing activity (n=6 mice per group). **(e-f)** Serum creatinine and blood urea nitrogen (BUN) after I/R-induced AKI (*Akr1a1*$^{+/+}$: 35 mice; *Akr1a1*$^{-/-}$: 36 mice; *Akr1a1*$^{-/-}$/*eNOS* $^{-/-}$: 13 mice; *eNOS*$^{-/-}$: 8 mice). X represents outlier. **(g)** H&E stain in injured kidneys. AKI-induced renal tubular injury includes severe tubular lysis (black arrow), loss of brush borders (green arrow) and sloughed debris in the tubular lumen (red arrow). Scale bars, 50μm. **(h)** Pathological scores of tubular injury (n=5 mice per group). **(i)** Survival curve following I/R-induced AKI. (n = 24 for *Akr1a1*$^{+/+}$ and 17 for *Akr1a1*$^{-/-}$; Gehan–Breslow–Wilcoxon test, P=0.0136). **(j)** Endogenous SNO-protein and iron nitrosyl (FeNO) levels in the mouse kidneys (n=6 mice per group). Results are presented as mean ± SD. One-way ANOVA with Tukey post hoc was used to detect significance in Fig.1e&f, 1h and 1j. Images in 1a-c, 1g and 1j are representative of two independently performed experiments with similar results. For gel source data, see Supplementary Figure 1.

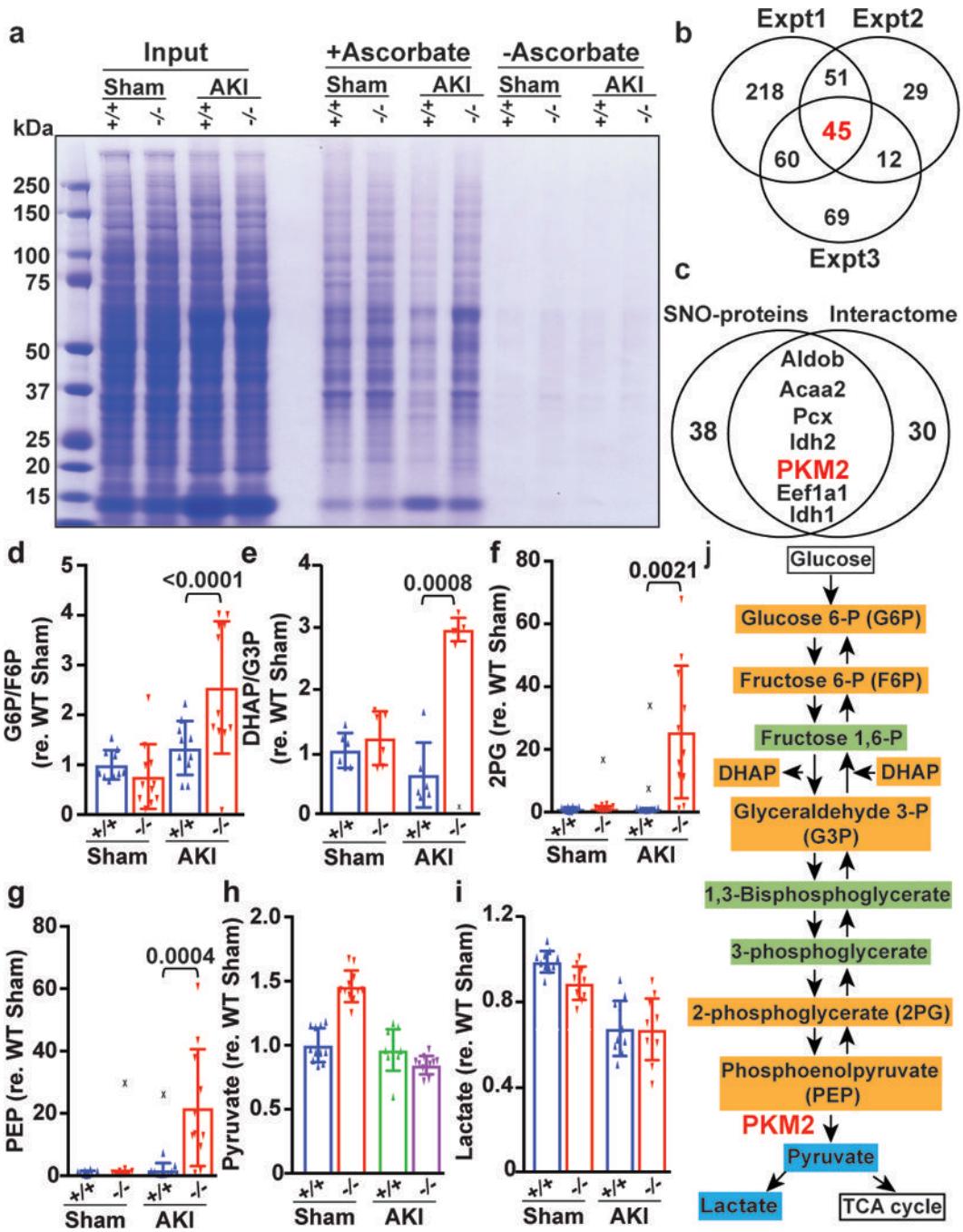

Figure 2. PKM2 is a major locus of regulation by the SNO-CoA/SCoR system.

(a) S-nitrosylated proteins (+Ascorbate) in the mouse kidneys. Image is representative of three independently performed experiments with similar results. –Ascorbate, control. **(b)** S-nitrosylated proteins enriched more than 1.4 fold in injured kidneys from *Akr1a1*$^{-/-}$ vs. injured kidneys from *Akr1a1*$^{+/+}$ mice in three independent experiments (SNO-RAC); injury induced by I/R. **(c)** Proteins found in both the S-nitrosoproteome in **b** (left circle) and AKR1A1 interactome (right circle) are labelled. **(d-i)** Glycolytic intermediates glucose 6-P (G6P), fructose 6-P (F6P), dihydroxyacetone phosphate (DHAP), glyceraldehyde 3-P (G3P),

2-phosphoglycerate (2PG), phosphoenolpyruvate (PEP), pyruvate and lactate (G6P/F6P, 2PG, PEP pyruvate and lactate: n=10 mice *Akr1a1*$^{+/+}$ group; n=11 mice per *Akr1a1*$^{-/-}$ group. DHAP/ G3P: n=6 mice per group). X represents outlier. **(j)** Glycolytic pathway metabolomics, comparing I/R-injured *Akr1a1*$^{+/+}$ vs. *Akr1a1*$^{-/-}$ mice. Intermediates in orange were increased, in blue were unchanged, in green were not identified. PKM2 enzyme is indicated in red.

Results are presented as mean ± SD. One-way ANOVA with Tukey post hoc was used for significance in Fig.1e-j.

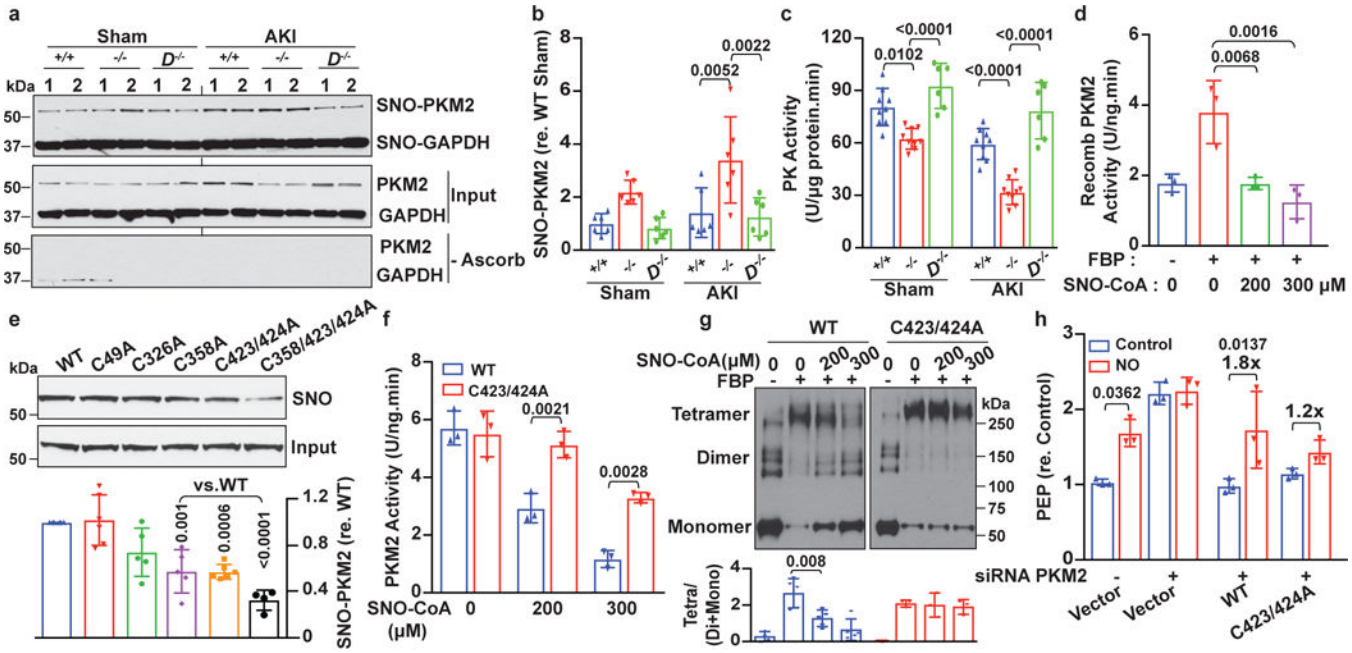

Figure 3. S-nitrosylation of renal PKM2 inhibits its activity by blocking tetramer formation.

(a) Endogenous S-nitrosylation (+Ascorbate) of PKM2. SNO-GADPH and GAPDH (input) are used as internal controls. Image is representative of two independently performed experiments with similar results. ($D^{-/-}$, *Akr1a1*$^{-/-}$/*eNOS*$^{-/-}$). **(b)** Quantification of SNO-PKM2. SNO is normalized to PKM2 (input; n=6 mice per group). **(c)** Activity of endogenous pyruvate kinase (PK) (n=9 mice per *Akr1a1*$^{+/+}$ or *Akr1a1*$^{-/-}$ group; n=6 mice per *Akr1a1*$^{-/-}$/*eNOS*$^{-/-}$ ($D^{-/-}$). **(d)** Activity of recombinant PKM2 proteins after SNO-CoA treatment (n=3 independent experiments). FBP=Fructose 1,6 biphosphate (PKM2 activator). **(e)** SNO in PKM2 cysteine mutants expressed in HEK cells (n=5 independent experiments). **(f)** Activity of recombinant PKM2-WT and PKM2-C423/424A after SNO-CoA treatment (n=3 independent experiments). **(g)** Dimer/tetramer distribution of recombinant PKM2-WT and PKM2-C423/424A after SNO-CoA treatment in vitro (n=5 independent experiments for PKM2-WT; n=3 independent experiments for PKM2-C423/424A). **(h)** Glycolytic intermediate accumulation (PEP) in Myc-PKM2-WT and Myc-PKM2-C423/424A expressing HEK cells after DETANO (NO) treatment (n=3 independent experiments). Results are presented as mean ± SD. One-way ANOVA with Tukey post hoc was used to detect significance in Fig.3b-h.

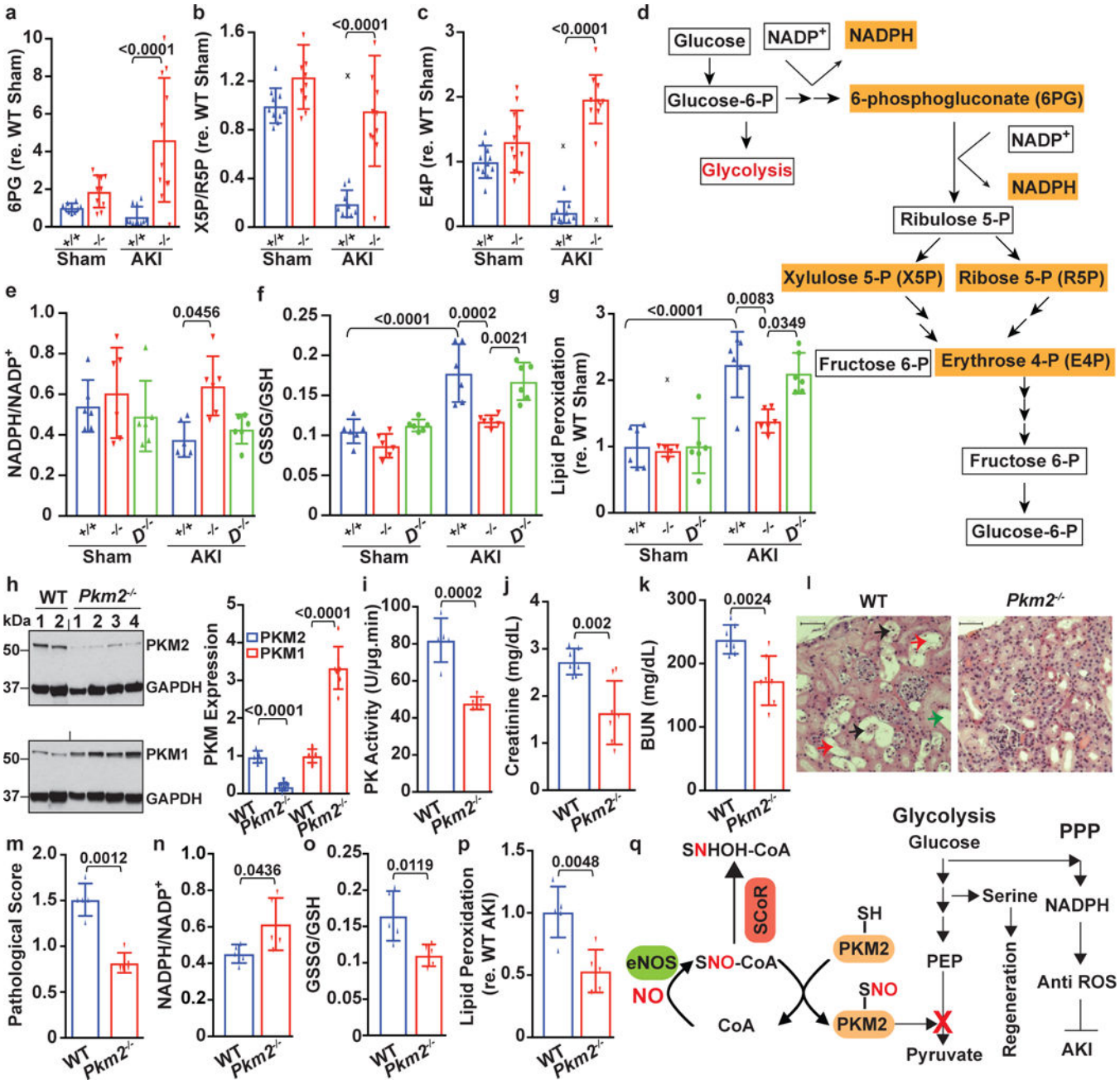

Figure 4. Inhibition of PKM2 by S-nitrosylation increases flux through the pentose phosphate pathway (PPP) and protects from AKI.

(a-c) Quantification of key PPP intermediates [6-phosphogluconate (6PG), xylulose 5-P (X5P), ribose 5-P (R5P), erythrose-4-phosphate (E4P)] (n=10 mice per *Akr1a1*$^{+/+}$ group; n=11 mice per *Akr1a1*$^{-/-}$ group). Injury induced with I/R. X represents outlier. **(d)** Pentose phosphate pathway. Intermediates in orange are increased. **(e-f)** Ratio of NADPH/NADP^{+} or GSSG/GSH (n=6 mice per group). Labels as in **1c**. **(g)** Lipid peroxidation (n=6 mice per group). **(h)** Expression of PKM2 and PKM1. Quantification is based on 5 mice per group. **(i)** Pyruvate kinase (PK) activity in kidneys (n=5 mice per group). **(j-k)** Serum creatinine and BUN after I/R-induced AKI (n=7 mice per group). **(l)** H&E staining in injured kidneys

(arrows; see 1g). Image is representative of two independently performed experiments with similar results. Scale bars, 50μm. **(m)** Pathological scores of tubular injury (n=5 mice per group). **(n-p)** NADPH/$NADP^+$, GSSG/GSH and lipid peroxidation (n=5 mice per group). **(q)** Working model showing how metabolic reprogramming by the SNO-CoA/SCoR system protects against kidney injury. Results are presented as mean ± SD. One-way ANOVA with Tukey post hoc was used to detect significance in Fig.4a-g. Two-tailed Student's t-test was used for significance in Fig.4h-k, 4m-p.